N78-78574

Copy number 13

Report number MDC A4816

DC-9 LANDING GEAR MATH MODEL FOR DIRECTIONAL CONTROL ON RUNWAY FLIGHT SIMULATION

Revision date

Revision letter

Issue date 19 May 1977

Contract number L-56926A

Prepared by Harry Passmore Chuck Korba

Harry Passmore, Section Chief
Flight Simulation

C. R. Korba, Engineer
Flight Simulation

Approved by Roger H Mathews

Roger H. Mathews
Chief Laboratory Engineer
Flight Simulation

REPRODUCED BY
NATIONAL TECHNICAL
INFORMATION SERVICE
U.S. DEPARTMENT OF COMMERCE
SPRINGFIELD, VA. 22161

MCDONNELL AIRCRAFT COMPANY

Box 516, Saint Louis, Missouri 63166 – Tel. (314)232–0232

MCDONNELL DOUGLAS

CORPORATION

90

TABLE OF CONTENTS

TABLE OF CONTENTS (Continued)

List Of Pages

LIST OF FIGURES

LIST OF FIGURES (Continued)

LIST OF TABLES

1.0 INTRODUCTION

During the Directional Control on the Runway (DCOR) simulation study conducted at McDonnell Aircraft Company in November 1974 and again in March 1976, the F-4 and DC-9 landing gear reactions were determined from an all digital subroutine LNDGR. The purpose of this subroutine was to calculate the gear reaction forces and moments imparted to the aircraft. These forces and moments were then used in conjunction with aerodynamic, propulsion and inertial forces and moments to determine the resulting dynamic motion of the aircraft.

The subject here is the development of the relations and integral equations that were programmed in this subroutine. Figure 1-1 is a diagram of the interrelations between the different aspects considered in the math model. Figures 1-2 through 1-6 depict detailed breakouts of the blocks outlined in Figure 1-1. These detailed blocks list the equation numbers, figure numbers and data source for the equations programmed in the LNDGR subroutine. The equation and figure numbers refer to expressions developed in subsequent sections of this report.

The charts of Figures 1-1 through 1-6 are intended to be sufficient for constructing a computer subroutine equivalent to the LNDGR routine developed at MCAIR, with reference to the body of the report for definitions and development. Due to the large number of operations that must be repeated for each landing gear system (nose, left main, right main), a subscript notation has been adopted in the report. The subscript j is used to indicate that the equations or terms must be considered as applying to all three gears. This permits the development of the relations in general terms without the necessity of repeating each expression three times. As an example, the term F_{j_S} used in equation (3.5-6) represents the force in the nose strut or the force in the left main gear strut or the force in the right main gear strut as the j is replaced by N(F_{NS}), L(F_{LS}) or R(F_{RS}) respectively. These terms are shown in Figure 1-3.

One further subscript notation has been used to simplify the expressions in the report. The subscript i is used to distinguish between the nose gear system and the main gear system for terms whose values for the left and right main gears are always the same. The i is replaced by N to indicate the nose gear, and by M to indicate the main gear. These terms are normally fixed data terms such as the linear damping coefficients for the nose gear C_{DN} or for the main gear C_{DM}.

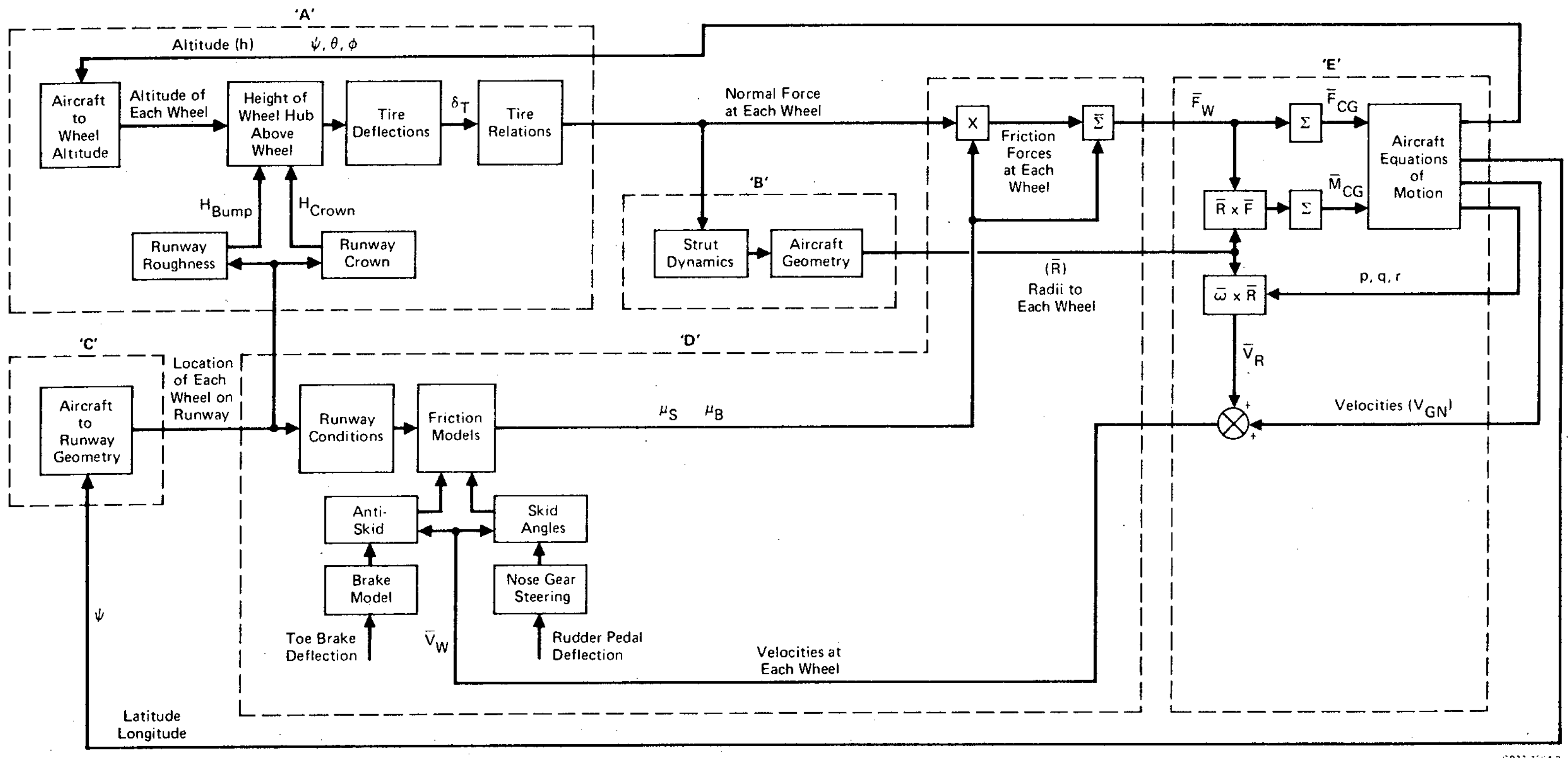

FIGURE 1-1
LANDING GEAR MATH MODEL SYSTEM DIAGRAM

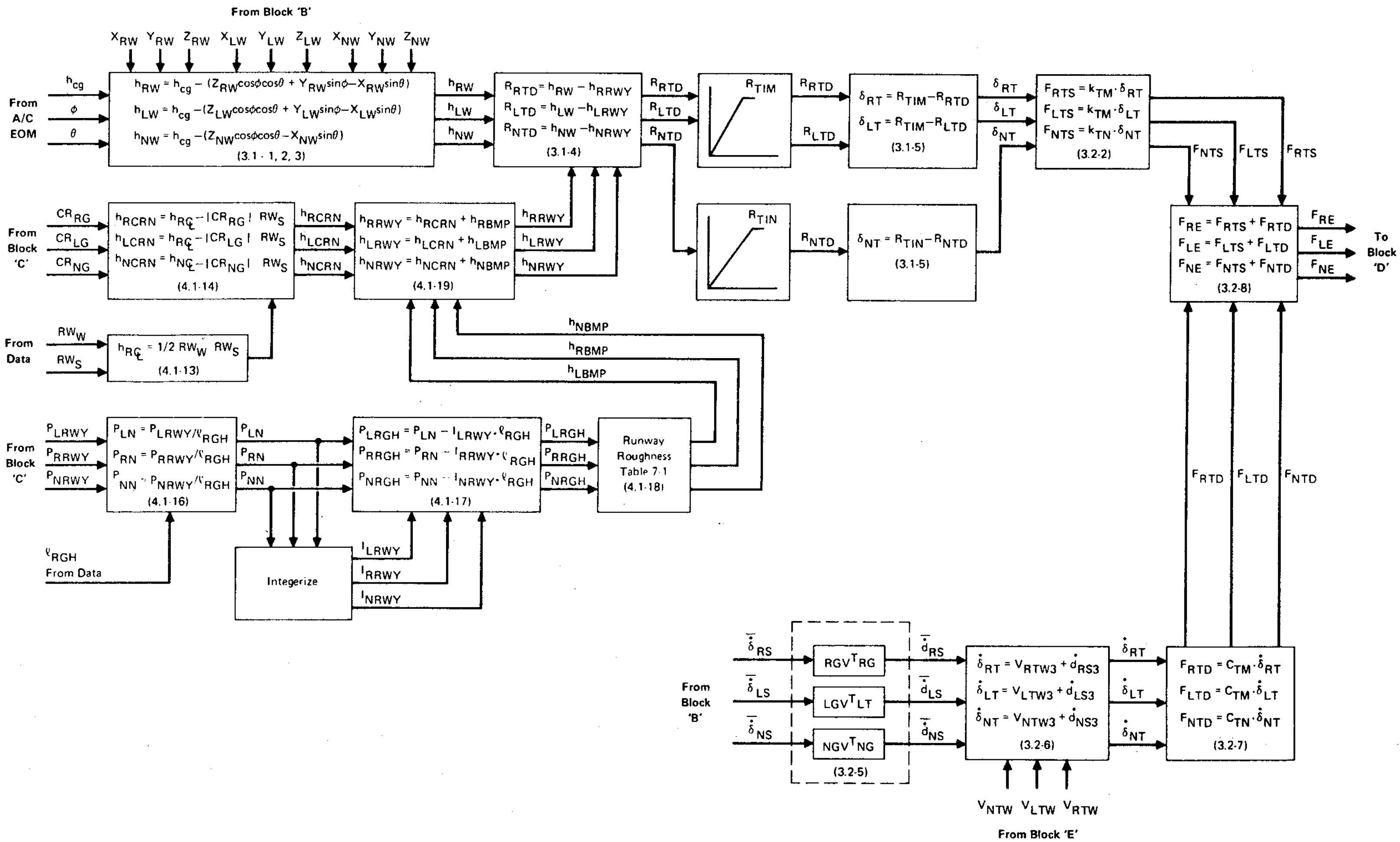

FIGURE 1-2
DETAILED BLOCK DIAGRAM 'A' - NORMAL WHEEL FORCE

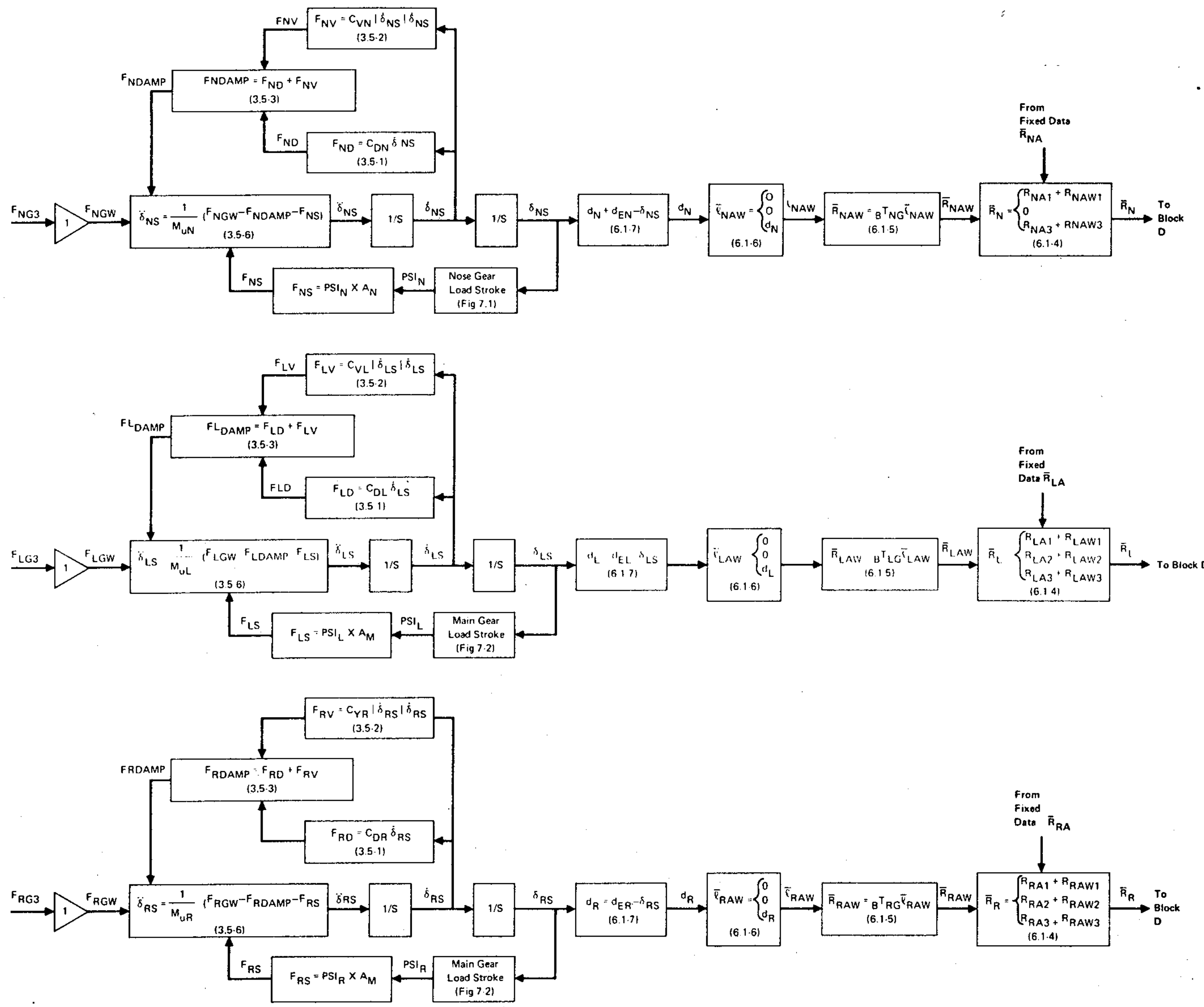

FIGURE 1-3
DETAILED BLOCK DIAGRAM 'B' - STRUT DYNAMICS

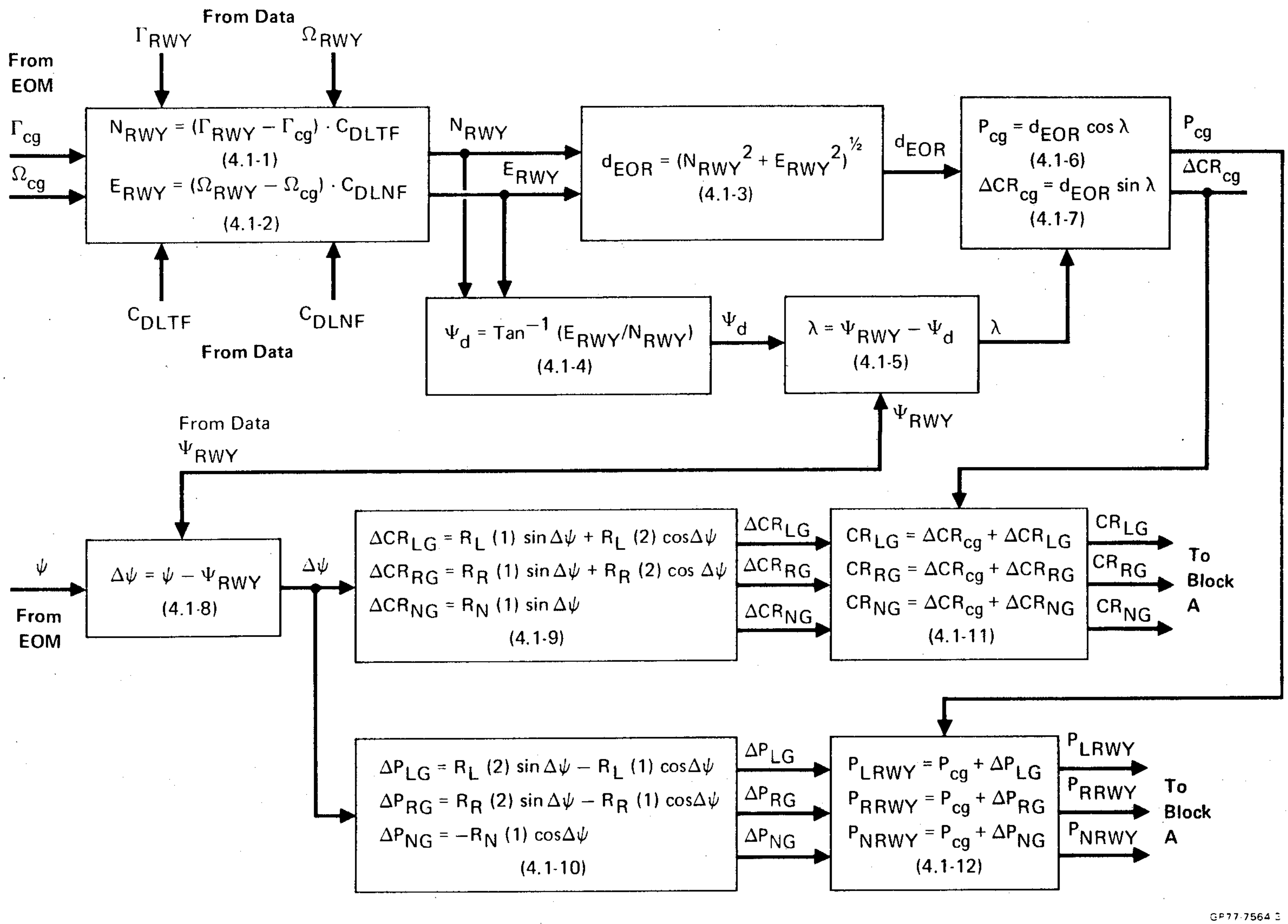

FIGURE 1-4
DETAILED BLOCK DIAGRAM 'C' - AIRCRAFT/RUNWAY GEOMETRY

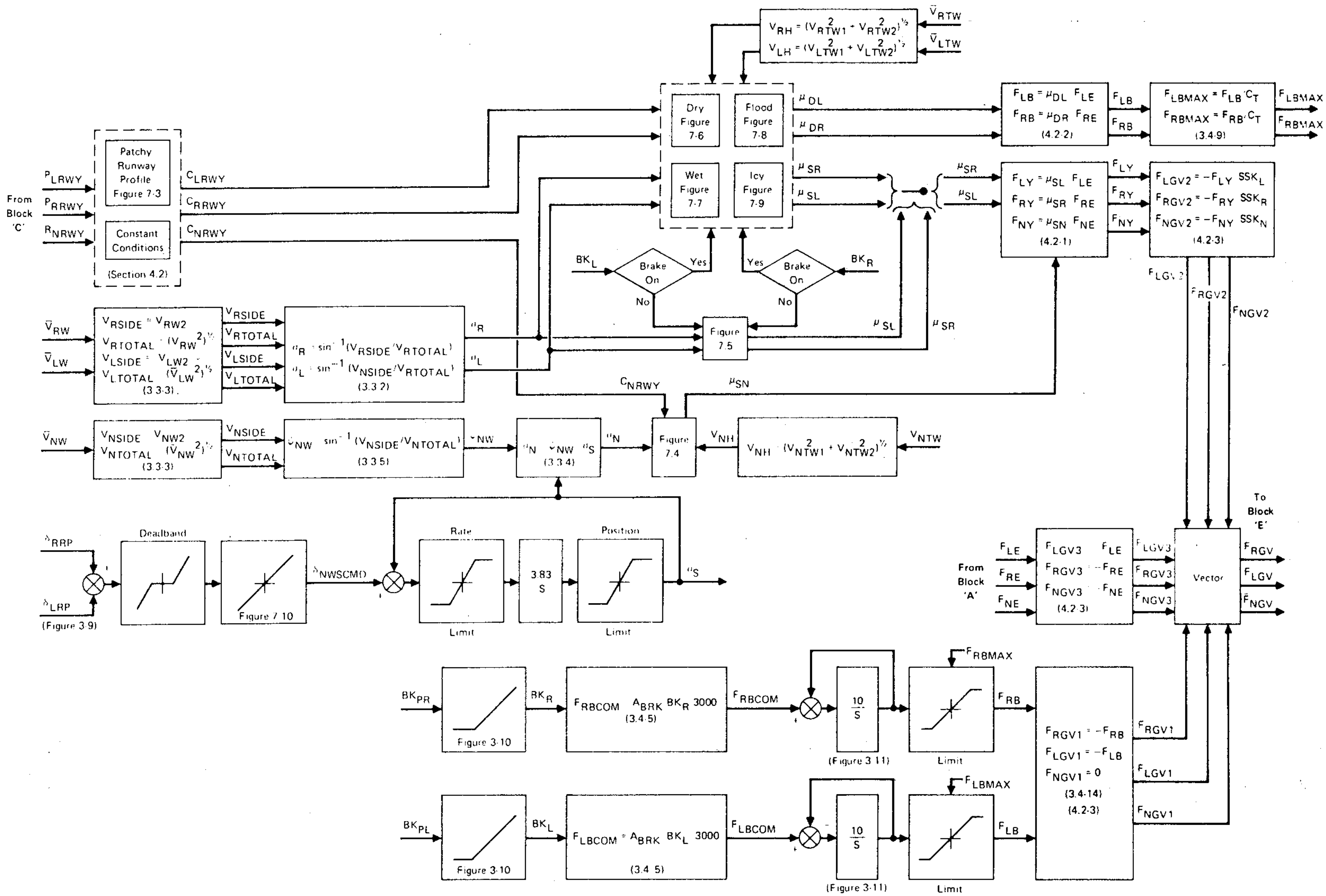

FIGURE 1-5
DETAILED BLOCK DIAGRAM 'D' - FRICTION FORCES

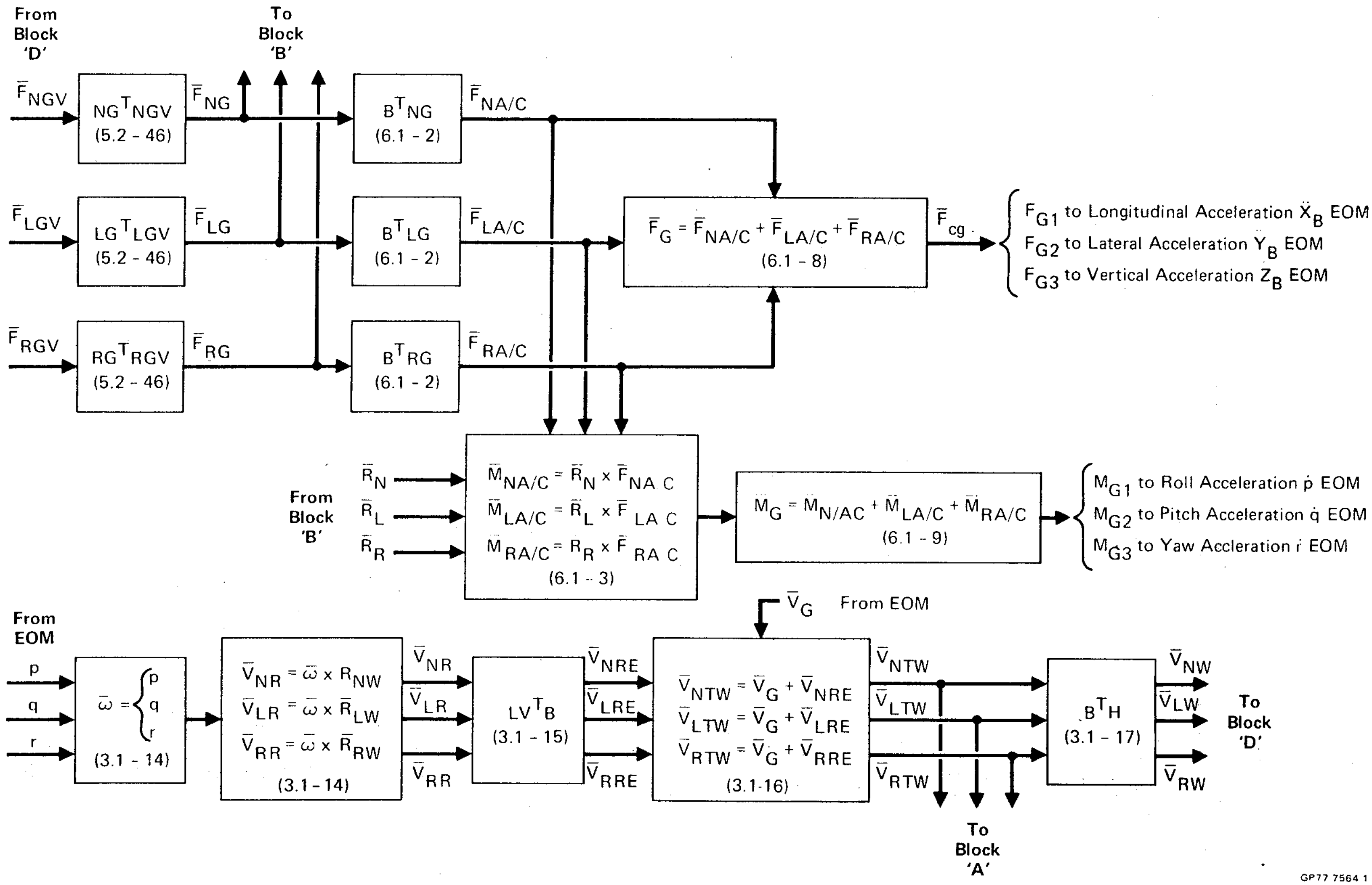

FIGURE 1-6
DETAILED BLOCK DIAGRAM 'E' WHEEL VELOCITIES AND OUTPUT

MCDONNELL DOUGLAS CORPORATION

MCDONNELL AIRCRAFT COMPANY

2.0 LIST OF SYMBOLS

The symbols are presented in two sections, engineering notation and Greek alphabet notation. The j and i subscript notation used in the report is followed in the list of symbols. These subscripts are ignored when establishing the alphabetical order of the list. All of the terms represented by the j or i are written in braces to the right of the symbol. However the definitions are only written one time for the basic symbol.

$$F_{js} \left\{ \begin{array}{l} F_{NS} \\ F_{LS} \\ F_{RS} \end{array} \right.$$

In addition, the components of a vector are written to the right of a vector symbol enclosed in parentheses.

$$\overline{X}\ (X_1, X_2, X_3)$$

If a vector term also includes a j or i subscript index, then the components of the general vector appear next to the symbol, with the vector terms identifying the index to the far right.

$$\overline{F}_{jG}\ (F_{jG1}, F_{jG2}, F_{jG3}) \left\{ \begin{array}{l} \overline{F}_{NG} \\ \overline{F}_{LG} \\ \overline{F}_{RG} \end{array} \right.$$

Throughout the report, a vector is denoted by a bar over the top of the symbol ($\overline{V}$). A dot above a symbol indicates the first derivative with respect to time and two dots indicate the second derivative with respect to time.

2.1 ENGINEERING SYMBOL/FORTRAN NOMENCLATURE

MATH MODEL SYMBOL	FORTRAN NAME	UNITS	DESCRIPTION
A			Subscript indicating gear attack points at the airframe; Hypothetical Axis System (Section 5.0)
A_{BRK}	ABRK	in^2	Effective braking area
A/C			Abbreviation for aircraft
A/C_{LAT}	ALAT		Latitude of the aircraft
A_{EA}			Auxiliary Euler angle for gear to body transformation
A_z		deg	Azimuth angle in the horizontal plane (Section 5.2.4)
B			Subscript indicating aircraft body axis system; Hypothetical Axis System (Section 5.0)
$BK_j \begin{cases} BK_L \\ BK_R \end{cases}$	BKLBDX BKRBDX	N/D	Normalized Toe Brake Deflection
C			Subscript indicating Hypothetical Axis System (Section 5.0)
$C_{Di} \begin{cases} C_{DN} \\ C_{DM} \end{cases}$	CMD	#/in/sec	Strut linear damping coefficient
C_{DLTF}	FTPDLA	ft/deg	Conversion factor degrees latitude to feet
C_{DLNF}	FTPDLP	ft/deg	Conversion factor degrees longitude to feet
c.g.	CG	%	Center of gravity
℄			Center Line
$C_{jP} \begin{cases} C_{LP} \\ C_{RP} \end{cases}$	PL PR	sec	Anti-skid cycling period

MATH MODEL SYMBOL		FORTRAN NAME	UNITS	DESCRIPTION
CP_G		CPG		Cozine of the gear longitudinal slant angle
CR_{jG}	CR_{NG}	DRCNW	ft	Distance from the runway centerline to a gear
	CR_{LG}	DRCLM		
	CR_{RG}	DRCRM		
C_{Ti}	C_{TN}	ACNT	#/in/sec	Tire linear damping coefficient
	C_{TM}	ACMT		
C_{jT}	C_{LT}	TIMONL	sec	Fraction of anti skid cycle time brake is on (Section 3.4)
	C_{RT}	TIMONR		
C_{Vj}	C_{VL}	CMVL	$\#/(in/sec)^2$	Strut velocity squared damping coefficient
	C_{VN}	CMVN		
	C_{VR}	CMVR		
C_{jYC}	C_{LYC}	CYCL	N/D	Anti-skid on/off cycle flag
	C_{RYC}	CYCR		
$C\theta$		CTH	N/D	Cosine of the pitch angle theta(θ)
$C\phi$		CPH	N/D	Cosine of the roll angle phi (ϕ)
$C\psi$		CSI	N/D	Cosine of the yaw angle psi (ψ)
$C_{11} - C_{33}$				General coefficients of a 3x3 matrix (Section 5.0)
D				Down component of the local Vertical axis system
d_{EOR}				Distance from end of the runway reference point to the c.g.
d_j	dN	DN	ft	Current strut length of the jth strut
	dL	DML		
	dR	DMR		
d_{iE}	dNE	DNE	ft	Extended strut length of the j^{th} strut
	dME	DME		

MATH MODEL SYMBOL	FORTRAN NAME	UNITS	DESCRIPTION
dt	CDT	sec	Differential time
E			East component of Local Vertical Axis System
EOM			Equations of Motion
EOR			End of the runway reference point
E_ℓ		deg	Elevation angle (Section 5.2.4)
E_{RWY}			Distance East from the c.g. to the runway longitude line.
F		lb	General force
$\overline{F}_{jA/C}(F_{jA/C1}, F_{jA/C2}, F_{jA/C3})$ $\overline{F}_{NA/C}$	FN		Force vector acting on the j^{th} gear in the Body Axis System
$\overline{F}_{RA/C}$	FMR		
$\overline{F}_{LA/C}$	FML		
F_{jB} { FLB, FRB		lb	Braking force
F_{jBAVG} { F_{RBAVG}, F_{LBAVG}			Braking force averaged over an anti-skid cycle period
F_{jBCOM} { F_{LBCOM}	FBLCOM	lb	Commanded braking force
F_{RBCOM}	FBRCOM		
F_{jBMAX} { F_{LBMAX}	FBRMAX	lb	Maximum braking force
F_{RBMAX}	FBLMAX		
F_{jBON} { F_{RBON}, F_{LBON}			Braking force applied during the brake-'on' portion of the anti-skid cycle period
F_{jD} { F_{ND}	FDN	lb	Strut linear damping force
F_{LD}	FDL		
F_{RD}	FDR		

MATH MODEL SYMBOL		FORTRAN NAME	UNITS	DESCRIPTION
F_{jDAMP}	F_{NDAMP}	FDAMPN	lb	Strut damping force
	F_{LDAMP}	FDAMPL		
	F_{RDAMP}	FDAMPR		
F_{jE}	F_{NE}	FNE	lb	Normal force acting on the tire at the ground
	F_{LE}	FLE		
	F_{RE}	FRE		
$\overline{F}_{jG}(F_{jG1}, R_{jG2}, F_{jG3})$	F_{NG}	FGN	lb	Force vector in the Gear axis system
	E_{RG}	FGMR		
	F_{LG}	FGML		
$\overline{F}_{jGV}(F_{jGV1}, F_{jGV2}, F_{jGV3})$	$\overline{F}_{NGV}$			Force Vector at the tire in the j^{th} gear velocity axis system
	$\overline{F}_{LGV}$			
	$\overline{F}_{RGV}$			
F_{jGW}	F_{NGW}		lb	Force from tire acting along the strut C_{L}
	F_{LGW}			
	F_{RGW}			
F_{jS}	F_{NS}	FSN	lb	Strut Spring force
	F_{RS}	FSL		
	F_{LS}	FSR		
F_{jTD}	F_{NTD}	FTVN	lb	Tire damping force
	F_{RTD}	FTVR		
	F_{LTD}	FTVL		
F_{jTS}	F_{NTS}	FTDN	lb	Tire spring force
	F_{LTS}	FTDL		
	F_{RTS}	FTDR		
F_{jV}	F_{NV}	FVN	lb	Strut velocity squared damping force
	F_{LV}	FVL		
	F_{RV}	FVR		

MATH MODEL SYMBOL		FORTRAN NAME	UNITS	DESCRIPTION
F_{jY}	$\left\{ \begin{array}{l} F_{NY} \\ F_{LY} \\ F_{RY} \end{array} \right.$		lb	Side force on the j^{th} wheel (Section 3.2.2)
h_{cg}		H	ft	Altitude of the aircraft measured at the c.g.
h_{jBMP}			ft	Height of the roughness bump at the wheel
h_{jCRN}		HCROWN	ft	Height of the runway crown at the wheel
h_{jRWY}			ft	Total height of the runway at the location of the j^{th} wheel
h_{jW}	h_{LW}	HUBHL	ft	Altitude of the j^{th} wheel hub
	h_{NW}	HUBHN	ft	
	h_{RW}	HUBHR	ft	
$h_{R℄}$			ft	Height of the runway crown at the centerline
i				Subscript index to indicate terms that differ between the nose and main gear systems.
I_{jRWY}				Index to indicate the section of the runway at each wheel (Section 4.1)
j				General subscript index to indicate to which particular gear a term applies
k_{Ti}	k_{TN}	AKNT	lb/in	Spring constant of the tire
	k_{TM}	AKMT		
L				subscript indicating left main gear

MATH MODEL SYMBOL	FORTRAN NAME	UNITS	DESCRIPTION
$\overline{\ell}$			General vector to a point (Section 5.2.4)
$\overline{\ell}_H$			Component of $\overline{\ell}$ projected into horizontal plane (Section 5.2.4)
$\overline{\ell}_{jAW}$			Vector from the j^{th} gear attach point to the wheel hub
$\overline{\ell}_{RGH}$		ft	Length of the section of roughness data
L_{RWY}		ft	Length of the runway
LV			Local Vertical axis system indicator
$\overline{\ell}_V$			Component of $\overline{\ell}$ projected into the vertical Y-Z plane (Section 5.2.4)
$\overline{M}_{jA/C}$ $\left\{ \begin{array}{l} \overline{M}_{LA/C} \\ \overline{M}_{NA/C} \\ \overline{M}_{RA/C} \end{array} \right.$	CGML CGMN CGMR	ft-lbs	Moment about the c.g. due to forces on the j^{th} gear
$\overline{M}_G$	GRMOM	ft-lbs	Total moment about the aircraft c.g. due to all gear forces
m_{uj}	USMN	slugs	Unsprung Mass (Section 3.0)
$\overline{N}$ (N,E,D.)			Vector in Local Vertical System with components North, East, Down
N.E.D.			North, East, Down designation for the Local Vertical axes
N_{RWY}		ft	Distance North from the c.g. to the end of runway reference point
p	p	rad/sec	Rate of aircraft angular rotation about the aircraft X_B axis

MATH MODEL SYMBOL	FORTRAN NAME	UNITS	DESCRIPTION
P_{cg}	DRTCG	ft	Distance along the runway from the EOR point to the c.g.
P_{iG} $\left\{ \begin{array}{l} P_{MG} \\ P_{NG} \end{array} \right.$	PG	deg	Angle between the aircraft station line and strut center line
P_{jN}			The number of data sectors between the j^{th} wheel location and the end of the runway
P_{jRGH}	PRWY	ft	The location of the j^{th} wheel within a roughness sector
P_{jRWY} $\left\{ \begin{array}{l} P_{NRWY} \\ P_{RRWY} \\ P_{LRWY} \end{array} \right.$	DRTNW DRTRM DRTLM	ft	Postion of the j^{th} gear on the runway
q	q	rad/sec	Rate of aircraft angular rotation about the aircraft $Y_{A/C}$ axis
R			Right gear indicator
r	r	rad/sec	Rate of angular rotation about the aircraft $Z_{A/C}$ axis.
$\bar{R}_{jA}(R_{jA1},R_{jA2},R_{jA3})$ $\left\{ \begin{array}{l} \bar{R}_{NA} \\ \bar{R}_{RH} \\ \bar{R}_{LA} \end{array} \right.$ $\{R_{MA}$	RNA RMRA RMLA		Radius vector from c.g. to attach point
$\bar{R}_{jAW}(R_{jAW1},R_{jAW2},R_{jA3})$ $\left\{ \begin{array}{l} \bar{R}_{NAW} \\ \bar{R}_{LAW} \\ \bar{R}_{RAW} \end{array} \right.$			Radius vector from attach point to wheel hub in body axes
$\bar{R}_j(R_j(1),\ R_j(2),R_j(3))$			Radius vector from A/C c.g. to the j^{th} wheel hub
R_{LG}	RLG	Deg	Angle the left main strut makes with A/C buttline

MATH MODEL SYMBOL	FORTRAN NAME	UNITS	DESCRIPTION
R_{RG}		deg	Angle the right main strut makes with A/C buttline
R_{jTD} $\left\{ \begin{array}{l} R_{NTD} \\ R_{LTD} \\ R_{RTD} \end{array} \right.$	RTDN RTDM	in	Deflected radius of a tire
R_{iTI} $\left\{ \begin{array}{l} R_{NTI} \\ R_{MTI} \end{array} \right.$	RTIN RTIM	in	Inflated radius of a tire
R_j			Radius vector from A/C c.g. to wheel hub
RWY			Abbreviation for Runway
RW_s		ft	Runway slope
RW_w		ft	Runway width
S			Laplace transform independent variable
SP_G	SPG	N/D	Sine of the strut angle P_G
SSK			Sign control term (Section 3.2)
S_θ	STH	N/D	Sine of the pitch angle θ
S_ϕ	SPH	N/D	Sine of the roll angle ϕ
S_ψ	SSI	N/D	Sine of the yaw angle ψ
t	TIME	sec	Time
td			Time at touchdown
${}_{A}T_{B}$			Transformation Matrix: System B to System A
${}_{B}T_{A}$			Transformation Matrix: System A to System B
${}_{B}T_{G}$			Transformation Matrix: Gear to A/C Body

MATH MODEL SYMBOL		FORTRAN NAME	UNITS	DESCRIPTION
${}_{B}T_{H}$				Transformation Matrix Horizontal plane to A/C Body
${}_{B}T_{I}$				Transformation Matrix Intermediate System to A/C Body
${}_{B}T_{jG}$	${}_{B}T_{LG}$, ${}_{B}T_{RG}$, ${}_{B}T_{NG}$			Transformation Matrix, j^{th} gear to A/C Body
${}_{B}T_{jGV}$	${}_{B}T_{LGV}$, ${}_{B}T_{RGV}$, ${}_{B}T_{NGV}$			Transformation Matrix, j^{th} gear velocity to A/C Body
${}_{C}T_{A}$				Transformation Matrix, System A to System C
${}_{C}T_{B}$				Transformation Matrix, System B to System C
${}_{H}T_{jGV}$				Transformation Matrix, j^{th} Gear Velocity to Horizontal
${}_{H}T_{LV}$				Transformation Matrix, Local Vertical to Horizontal
${}_{I}T_{H}$				Transformation Matrix, Horizontal to Intermediate
${}_{I}T_{LG}$				Transformation Matrix, Left Gear to Intermediate
${}_{jG}T_{B}$	${}_{NG}T_{B}$, ${}_{RG}T_{B}$, ${}_{LG}T_{B}$			Transformation Matrix, A/C Body to j^{th} Gear
${}_{JG}T_{H}$	${}_{NG}T_{H}$, ${}_{LG}T_{H}$, ${}_{RG}T_{H}$			Transformation Matrix, Horizontal to j^{th} Gear
${}_{jG}T_{jGV}$	${}_{NG}T_{NGV}$, ${}_{RG}T_{RGV}$, ${}_{LG}T_{LGV}$			Transformation Matrix, j^{th} Gear Velocity to j^{th} Gear

MATH MODEL SYMBOL		FORTRAN NAME	UNITS	DESCRIPTION
$\overline{V}$ (V1,V2,V3)			ft/sec	Vector in special axis System B (Section 5.0)
$\overline{V}_G$ (V_{G1},V_{G2},V_{G3})		VGN	ft/sec	A/C velocity vector in Local Vertical System
$\overline{V}_{jR}$ $(V_{jR1},V_{jR2},V_{jR3})$	$\overline{V}_{NR}$ $\overline{V}_{LR}$ $\overline{V}_{RR}$		ft/sec	Velocity vector at wheel due to A/C rotations, Body System
$V_{jRE}(V_{jRE1},V_{jRE2},V_{jRE3})$	VNRE VLRE VRRE	VNWE VLWE VRWE	ft/sec	Velocity vector at wheel due to A/C rotations, LV system
V_{jSIDE}	V_{NSIDE} V_{LSIDE} V_{RSIDE}	VSIDEN	ft/sec	Side velocity at the gear (Section 3.2)
V_{jTOTAL}	V_{NTOTAL} V_{RTOTAL} V_{LTOTAL}	VTNW	ft/sec	Total velocity at the gear (Section 3.2)
$\overline{V}_{jTW}$ $(V_{jTW1},V_{jTW2},V_{jTW3}0$	$\overline{V}_{NTW}$ $\overline{V}_{LTW}$ $\overline{V}_{RTW}$		ft/sec	Total velocity vector at the wheel, LV system
$\overline{V}_{jW}$ $(V_{jW1},V_{jW2},V_{jW3})$	$\overline{V}_{LW}$ $\overline{V}_{RW}$ $\overline{V}_{NW}$		ft/sec	Total velocity vector at the wheel, A/C body system
W_{Ti} (W_{TM},W_{TN})		WTM WTN	lb	Unsprung Weight

MATH MODEL SYMBOL	FORTRAN NAME	UNITS	DESCRIPTION
$\overline{X}(X1,X2,X3)$			Vector in hypothetical system A (Section 5.0)
X			Longitudinal component of a general axis system (Section 5.1)
x			Component of $\overline{\ell}$ along X (Section 5.2.4)
$\overline{X}_B(XB,XB,ZB)$			Vector in the Aircraft Body System
$\overline{X}_{jG}(X_{jG},Y_{jG},Z_{jG})$, $\begin{cases}\overline{X}_{LG}\\ \overline{X}_{RG}\\ \overline{X}_{NG}\end{cases}$			Vector in Gear Axis System
$\overline{X}_H(X_H,Y_H,Z_H)$			Vector in Horizontal axis system
$\overline{X}_I(X_I,Y_I,Z_I)$			Vector in Intermediate axis system
$\overline{X}_{jGV}(X_{jGV},Y_{jGV},Z_{jGV})$ $\begin{cases}\overline{X}_{NGV}\\ \overline{X}_{LGV}\\ \overline{X}_{RGV}\end{cases}$			Vector in the j^{th} Gear Velocity axis system
X_{MG}		ft	Distance from A/C c.g. to Main gear (Figure 3-3)
X_{NG}		ft	Distance from A/C c.g. to Nose gear (Figure 3-3)
Y			Lateral component of a general axis system (Section 5.1)
y			Component of $\overline{\ell}$ along Y (Section 5.2.4)

MATH MODEL SYMBOL		FORTRAN NAME	UNITS	DESCRIPTION
Y_B				Lateral component of $\overline{X}_B$
Y_{jG}	Y_{NG}, Y_{RG}, Y_{LG}			Lateral component of $\overline{X}_{jG}$
Y_H				Lateral component of $\overline{X}_H$
Y_I				Lateral component of $\overline{X}_I$
Y_{jGV}	Y_{NGV}, Y_{RGV}, Y_{LGV}			Lateral component of $\overline{X}_{jGV}$
Y_{LW}			ft	Lateral distance to left wheel from Aircraft centerline
Y_{RW}			ft	Lateral distance to right wheel from aircraft centerline
Z				Down component of a general axis system
z				Projection of $\overline{\ell}$ vector along Z axis (Section 5.2.4)
Z_B				Down component of $\overline{X}_B$
Z_{jG}	Z_{NG}, Z_{LG}, Z_{RG}			Down component of $\overline{X}_G$
Z_H				Down component of $\overline{X}_H$
Z_I				Down component of $\overline{X}_I$

MATH MODEL SYMBOL		FORTRAN NAME	UNITS	DESCRIPTION
Z_{jGV}	Z_{NGV}, Z_{LGV}, Z_{RGV}			Down component of $\overline{X}_{jGV}$
Z_{MW}			ft	Distance from A/C centerline down to Main wheel
Z_{NW}			ft	Nose wheel
Z_{RW}			ft	Distance along Z_B from A/C centerline to Right wheel
Z_{LW}			ft	Distance along Z_B from A/C centerline to left wheel

2.2 GREEK SYMBOLS

ΔCR_{cg}		DRCCG	ft	Lateral distance from runway centerline to aircraft c.g.
ΔCR_{jG}	ΔCR_{NG}, ΔCR_{RG}, ΔCR_{LG}	DRCNW, DRCRM, CRCLM	ft	Lateral distance from aircraft c.g. to gear
ΔP_{jG}	ΔP_{NG}, ΔP_{LG}, ΔP_{RG}		ft	Distance along the runway from the c.g. to the j^{th} gear
$\Delta\psi$				Difference between the Euler yaw angle ψ and the heading of the runway
δ_{jS}	δ_{NS}, δ_{LS}, δ_{RS}			Deflection of the j^{th} strut
δ_{jStd}	δ_{NStd}, δ_{RStd}, δ_{LStd}	DEFN, DEFR, DEFL	ft	Deflection of the j^{th} strut at touchdown

MATH MODEL SYMBOL		FORTRAN NAME	UNITS	DESCRIPTION
δ_{NWSCMD}		STRCOM	deg	Commanded Nose wheel steering angle
δ_{jT}	δ_{NT}	DELTN	in	Tire deflection
	δ_{LT}	DELTL		
	δ_{RT}	DELTR		
θ		THA	deg	Euler pitch angle of the aircraft
μ_{jB}				Braking coefficient of friction with brake-'on'
μ_{jD}	μ_{LD}	COFRBL	N/D	Braking coefficient of friction with anti-skid operating
	μ_{RD}	COFRBR		
μ_{jS}	μ_{NS}	COFRSN	N/C	Side force coefficient of friction
	μ_{LS}	COFRSL		
	μ_{RS}	COFRSR		
Σ				Summation symbol
$\overline{\Sigma}$				Components are summed into a vector
σ_j	σ_N	SKANGN	deg	Skid angle
	σ_L	SKANGL		
	σ_R	SKANGR		
σ_s		STRANG	deg	Nose wheel steering angle
ϕ		PHI	deg	Euler Roll angle
ψ		PSI	deg	Euler Yaw angle
Ψ_d				Angle between N_{RWY} and d_{EOR}
ψ_{jW}	ψ_{NW}		deg	Angle between the velocity vector at the j^{th} wheel and the longitudinal axis X_H in the horizontal axis system
	ψ_{LW}			
	ψ_{RW}			

MATH MODEL SYMBOL	FORTRAN NAME	UNITS	DESCRIPTION
ψ_{RWY}			Heading of the runway from North
λ		deg	Angle between d_{EOR} and the runway ℄
γ		deg	Elevation of the projected vector $\overline{\ell}_V$ (Figure 5-11)
Γ_{cg}		deg	Latitude of the A/C at the c.g.
Γ_{RWY}		deg	Latitude of the EOR reference point
Ω_{cg}		deg	Longitude of the A/C at the c.g.
Ω_{RWY}		deg	Longitude of the EOR reference point
$\overline{\omega}$ (p,q,r)		rad/sec	Aircraft rotational velocity vector with components p,q,r along the X_B,Y_B and Z_B axes respectively.

3.0 DEVELOPMENT OF EQUATIONS

Each landing gear is considered to consist of an oleo strut and a tire as depicted in Figure 3-1.

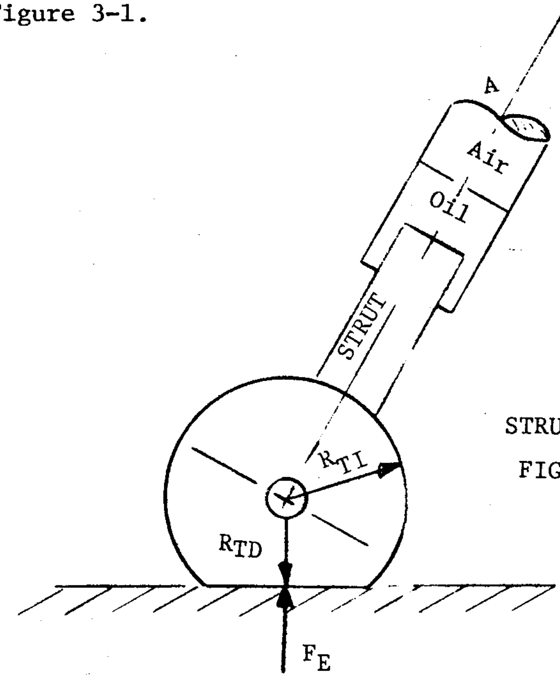

STRUT AND TIRE
FIGURE 3-1

This system imparts a force, which is a function of the gear reactions, on the aircraft at the gear attachment point A. To calculate these forces, both the tire and the strut are treated as simplified spring, mass, damper systems. The model used for the tire is shown in Figure 3-2.

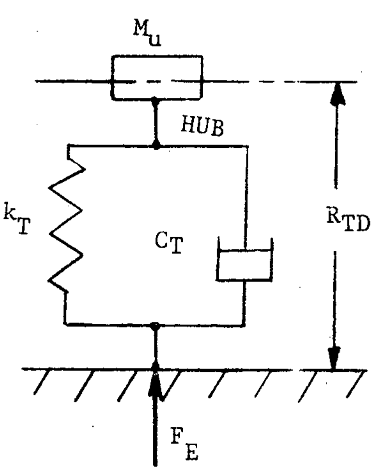

TIRE
SPRING-MASS-DAMPER

FIGURE 3-2

The velocity at each wheel is used to determine the skid angles between the wheels and the direction of travel. These angles are used to establish the coefficients of braking and skidding friction between the wheel and the runway.

3.1 AIRCRAFT AND WHEEL HEIGHT GEOMETRY

The geometrical relations of the aircraft's orientation are used to determine the height of the hub of each wheel above the runway. Figure 3-3 depicts the gear geometry nomenclature to be used. R_{MA1}, R_{MA2} and R_{MA3} are the longitudinal, lateral and vertical locations of the main gear attachment points as measured from the center of gravity (c.g.). R_{NA1}, R_{NA2}, and R_{NA3} are the respective measurements to the nose gear attachment points. P_{MG} is the angle the main gear makes with the aircraft stationline. P_{NG} is the angle the nose gear makes with the stationline. R_{LG} is the angle the left main gear makes with the aircraft buttline measured positive for gear extending outboard. R_{RG} (not shown) is the angle the right main gear makes with the aircraft buttline. It is the negative of R_{LG}.

The wheels are located with respect to the c.g. by the distances along the aircraft body axes. The longitudinal distance from the c.g. to the nose wheel is X_{NG}. The longitudinal distance from the c.g. to the main wheels is X_{MG}. This value is negative as shown in the figure when the wheel is aft of the c.g. Also, the value of X_{MG} may be different for the left main gear and the right main gear when the gear struts are compressed different amounts and the angle P_{MG} is not zero. The distance from the aircraft's centerline down to the nose wheel is Z_{NW}. The distance down to the main wheel is Z_{MW}. Again, Z_{MW} may differ for the left and right gears when they are compressed. Y_{RW} is the positive distance from the centerline (zero buttline) to the right main wheel: Y_{LW} is the negative distance to the left main wheel. The nose wheel is located on the zero buttline.

To determine the height of a wheel (actually the wheel hub) above the ground, consider the geometry of Figure 3-4. This figure depicts the ground plane and a parallel plane X_H-Y_H through the c.g. of the aircraft. The aircraft axis system X,Y,Z intersects the X_H-Y_H plane at the c.g. The X-Y plane intersects the vertical X_H-Z_H plane at an angle θ (known as the pitch angle); and intersects the lateral Y_H-Z_H plane at an angle ϕ, known as the roll angle.

Considering the right main wheel only, the diagram depicts the projection of each component of the wheel location along each aircraft body axis X_{MG}, Aircraft Geometry

FIGURE 3-3

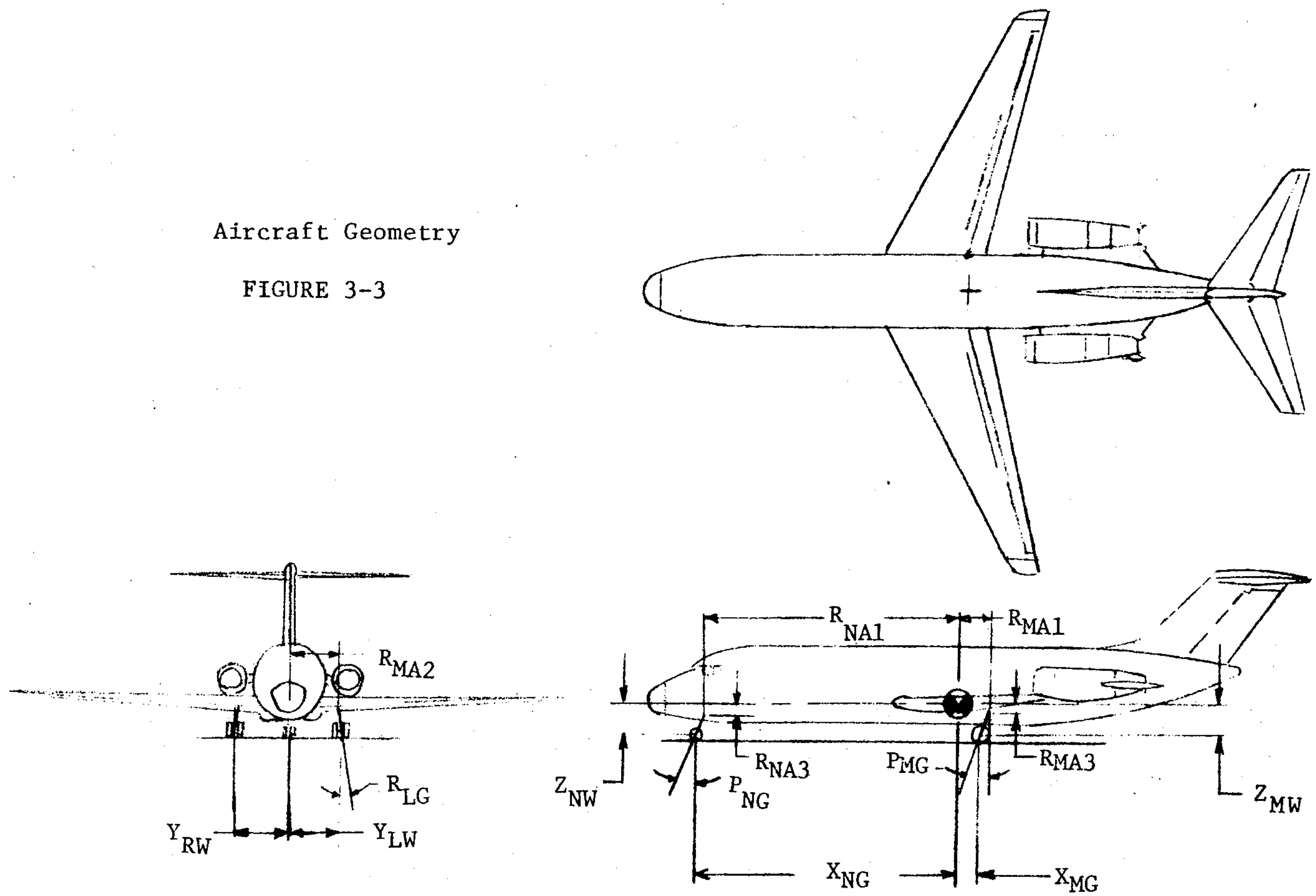

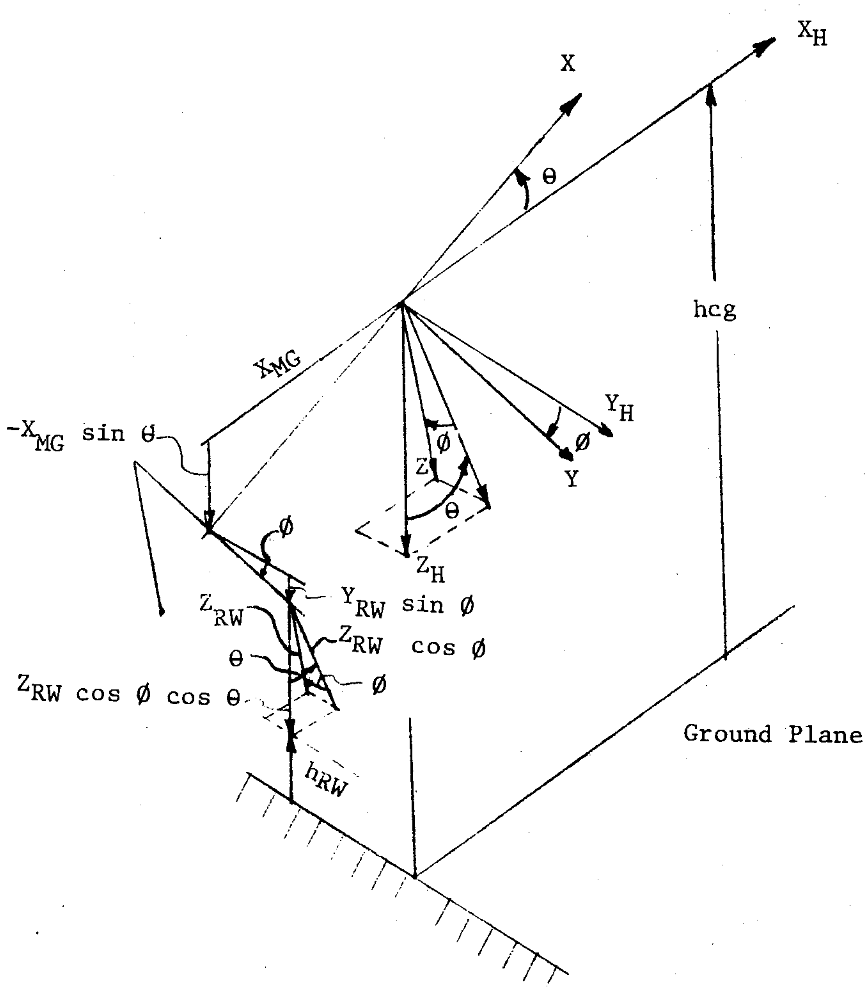

WHEEL HEIGHT GEOMETRY

FIGURE 3-4

Y_{RW}, Z_{RW} into the vertical direction. The height of the wheel hub above the ground plane is then seen to be the height of the c.g. above the ground plane less the sum of the vertical projections.

$$h_{RW} = h_{cg} - (Z_{RW} \cos \phi \cos \theta + Y_{RW} \sin \phi - X_{MG} \sin \theta) \qquad (3.1\text{-}1)$$

Similar relations may be developed for the left main and nose gear

$$h_{LW} = h_{cg} - (Z_{LW} \cos \phi \cos \theta + Y_{LW} \sin \phi - X_{MG} \sin \theta) \qquad (3.1\text{-}2)$$

$$h_{NW} = h_{cg} - (Z_{NW} \cos \phi \cos \theta - X_{NG} \sin \theta) \qquad (3.1\text{-}3)$$

When the tire is touching the runway, the tire is compressed. The distance between the hub of the wheel and the runway surface is called the deflected tire radius, R_{jTD}, as shown in Figure 3-1. This radius is determined for each tire as the difference between the height of the wheel hub above ground level, from the appropriate equation 3.1-1, 3.1-2 or 3.1-3, and the height of the runway at each wheel above ground level as determined from equation 4.1-9.

$$R_{jTD} = h_{jW} - h_{jRWY} \qquad (3.1\text{-}4)$$

The deflection of the tire is then the difference between the tire radius when fully inflated, R_{TI}, and the current tire radius.

$$\delta_{jT} = R_{iTI} - R_{jTD} \qquad (3.1\text{-}5)$$

These deflections and rates of deflection are then used to determine the normal force between the tire and the ground F_{jE}.

The normal force is used in conjunction with the friction coefficients to establish forces along and perpendicular to the velocity vector at each wheel. These three forces then comprise a force vector in an axis system oriented with the velocity at the wheel. This force vector $\overline{F}_{jGV}$ is then transformed into a force system aligned with and normal to the longitudinal axis of the gear. Through the transformation ${}_{jG}T_{jGV}$

$$\overline{F}_{jG} = {}_{jG}T_{jGV}\overline{F}_{jGV} \qquad (3.1\text{-}6)$$

These force systems are shown in Figure 3-5.

For this development, the forces normal to the strut that would result in bending in the strut have been neglected. The force along the strut longitudinal axis, F_{jG3}, is used in conjunction with the forces in the strut that result from spring compression.and damping to calculate the acceleration of the unsprung mass.

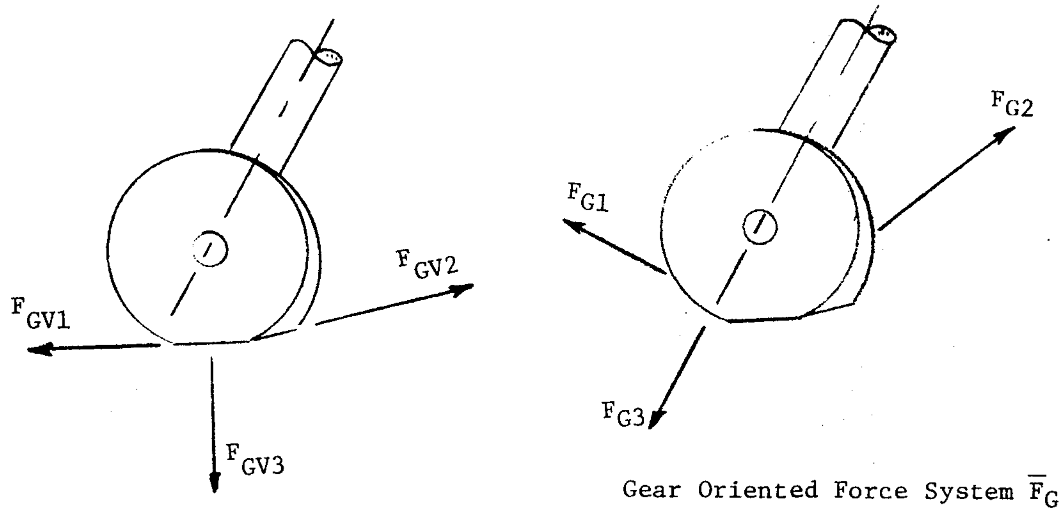

Velocity Oriented Force System $\overline{F}_{GV}$

Gear Oriented Force System $\overline{F}_G$

Figure 3-5

$$\ddot{\delta}_{js} = \frac{\overline{\Sigma F}}{m_{uj}} \tag{3.1-7}$$

where m_{uj}, the unsprung mass, represents the combined mass of the strut, wheel and tire. This acceleration is then integrated to obtain the rate of compression

$$\dot{\delta}_{js} = \dot{\delta}_{js_{td}} + \int_{td}^{t} \ddot{\delta}_{js}\, dt \tag{3.1-8}$$

and the compression of the strut.

$$\delta_{js} = \dot{\delta}_{js_{td}} + \int_{td}^{t} \dot{\delta}_{js}\, dt \tag{3.1-9}$$

The current strut length d_j is calculated as the extended strut length, d_{iE}, less the deflection.

$$d_j = d_{iE} - \delta_{js} \tag{3.1-10}$$

The vector distance from the gear attach points to the wheels may be formulated as

$$\overline{\ell}_{jAW} = \begin{Bmatrix} o \\ o \\ dj \end{Bmatrix} \tag{3.1-11}$$

The current strut length is added to the fixed distance from the center of gravity (c.g.) to the gear attach point, $\overline{R}_{jA}$, to establish the present value of the components of the radius vector from the c.g. to the wheel. The components of $\overline{R}_{jAW}$ along the aircraft body axes may be determined by transforming the vector $\overline{\ell}_{jAW}$ from gear to body axes.

$$\overline{R}_{jAW} = B^T G \quad \overline{\ell}_{jAW} \tag{3.1-12}$$

Then the radius to each wheel from the c.g. may be expressed

$$\overline{R}_{jW} = \overline{R}_{jA} + \overline{R}_{jAW} \tag{3.1-13}$$

The velocity at the wheel due to aircraft body rotations is calculated by the cross product

$$\overline{V}_{jR} = \overline{\omega} \times \overline{R}_{jW} \tag{3.1-14}$$

where $\overline{\omega}$ has the components, p,q and r about the aircraft X, Y and Z body axes respectively. These velocity components are transformed to a local vertical (North, East, Down) axis system.

$$\overline{V}_{jRE} = {}_{LV}{}^{T}{}_{B} \cdot \overline{V}_{jR} \tag{3.1-15}$$

The total velocity at the wheel is obtained by adding the velocity of the aircraft to these rotational components.

$$\overline{V}_{jTW} = \overline{V}_G + \overline{V}_{jRE} \tag{3.1-16}$$

A final transformation orients the velocity components in the horizontal plane to the aircraft body.

$$\overline{V}_{jW} = B^T H \; \overline{V}_{jTW} \tag{3.1-17}$$

The horizontal plane components of $\overline{V}_{jW}$ are used to determine the skid angles of the tires.

3.2 TIRE DYNAMICS

The dynamic model of the aircraft tire is developed by representing the tire as a simple spring, mass damper system shown in Figure 3-6.

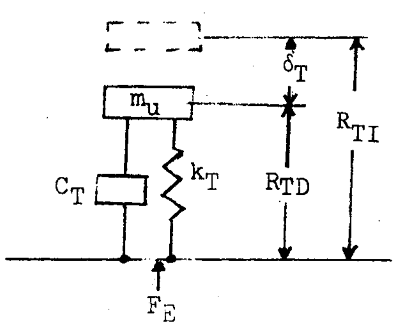

Aircraft Tire Dynamic Model

Figure 3-6

The normal force placed on the tire at the ground is reacted by the forces in the deflected spring and damper system. As previously expressed, the tire deflection is the difference between the inflated radius of the tire R_{iTI} and the current radius, R_{jTD}, which represents the height of the hub above the local runway level.

$$\delta_{jT} = R_{iTI} - R_{jTD} \tag{3.2-1}$$

Assuming the tire operates within the linear region of the spring, the spring force in the tire is obtained from

$$F_{jTS} = k_{Ti}\ \delta_{jT} \tag{3.2-2}$$

where k_{TI} is the spring constant of the tire.

The rate of compression $\dot{\delta}_{jT}$ of the tire is the sum of the downward components of the downward components of two velocity vectors. The first is V_{jTW3}, the downward component of the total rigid aircraft velocity at the wheel from equation 3.1-16. The second is the downward component of the compression rate of the strut. This term is obtained by first constructing a vector in the gear axis system with $\dot{\delta}_{js}$ of equation 3.1-8 as the third component

$$\bar{\dot{\delta}}_{js} = \left.\begin{matrix} 0 \\ 0 \\ \dot{\delta}_{js} \end{matrix}\right\} \tag{3.2-3}$$

The downward component of the strut rate is then the third component $\bar{\dot{d}}_{js3}$ formed by transforming $\bar{\dot{\delta}}_{js}$ from the gear axis system to the gear velocity axis system using the inverse of the transformation developed in Section 5.2.7.

$$_{jGV}T_{jG} = {_{jG}T_{jGV}}^{-1} \tag{3.2-4}$$

Then $$\bar{\dot{d}}_{js} = {_{jGV}T_{jG}}\ \bar{\dot{\delta}}_{js} \tag{3.2-5}$$

Finally, the rate of compression of the tire may be expressed

$$\dot{\delta}_{jT} = V_{jTW3} + \dot{d}_{jS3} \tag{3.2-6}$$

The damping in the tire is taken to be viscous; hence the force in the tire is given as the linear expression

$$F_{jTD} = C_{Ti} \quad \dot{\delta}_{jT} \tag{3.2-7}$$

where C_{Ti} is the damping coefficient of the "dashpot" damper.
The force between the tire and the ground acts normal to the ground plane and is equal in magnitude to the sum of the two reactive forces of the tire

$$F_{jE} = F_{jTS} + F_{jTD} \tag{3.2-8}$$

and

$$F_{jGV3} = -F_{jE} \tag{3.2-9}$$

3.3 CORNERING FORCES

Cornering forces are those forces which act on the tire to make it turn or change its direction of motion. To change the direction of motion or velocity of a tire, an acceleration, and hence a force, normal to the current direction must be applied to the tire. This cornering force is a function of the coefficient of cornering friction between the tire and the runway surface and the normal force acting on the tire.

$$F_{jGV2} = -\mu_{js} \cdot F_{jE} \cdot SSK \tag{3.3-1}$$

where μ_{js} is the coefficient of skidding or cornering friction at the wheel and SSK is a term whose value is 1 and whose sign is the same as the sign of the skid angle. This insures that the calculated force opposes the skid.

3.3.1 Skid Angles.

The angle between the rolling plane of the tire and the direction of the velocity vector in the horizontal plane is defined as the skid angle σ as shown in Figure 3-7.

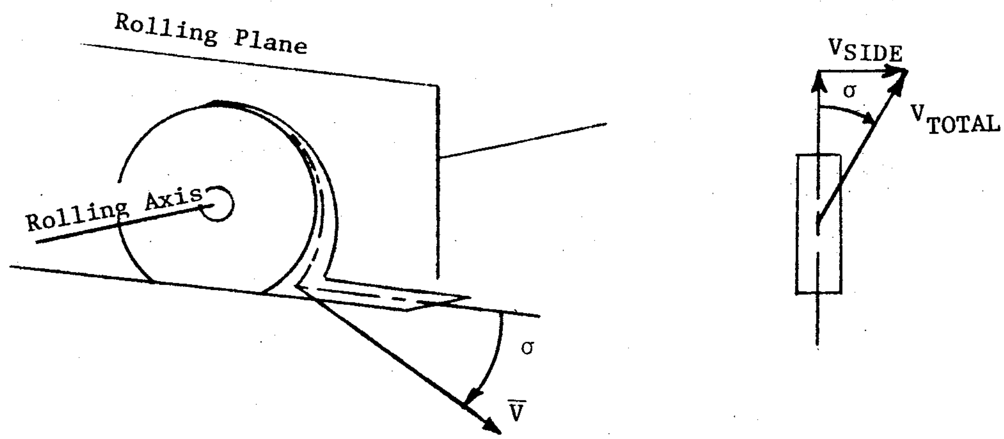

Skid Angle

Figure 3-7

To calculate this angle, the velocity of the tire must be expressed in terms of its components in and perpendicular to the rolling plane. The skid angle σ is then

$$\sigma = \sin^{-1} (V_{jSIDE}/V_{jTOTAL}) \tag{3.3-2}$$

The main gear tires are assumed to remain aligned with the aircraft body X-axis (buttlines). The velocity component V_{jSIDE} is then the second component of the aircraft oriented wheel velocity $\overline{V}_{jW}$ defined in equation (3.1-17).

$$V_{jSIDE} = V_{jW2} \tag{3.3-3}$$

The nose wheel presents a different picture however, for the rolling plane of the nose wheel may be offset from the aircraft buttline by a pilot induced nose wheel steering angle. Defining Ψ_{NW} as the angle between the velocity vector and the aircraft longitudinal axis, and σ_s as the pilot induced nose wheel steering angle; it is seen from Figure 3-8 that the skid angle is

$$\sigma_N = \Psi_{NW} - \sigma_s \tag{3.3-4}$$

where now

$$\Psi_{NW} = \sin^{-1} (V_{NSIDE}/V_{NTOTAL}) \tag{3.3-5}$$

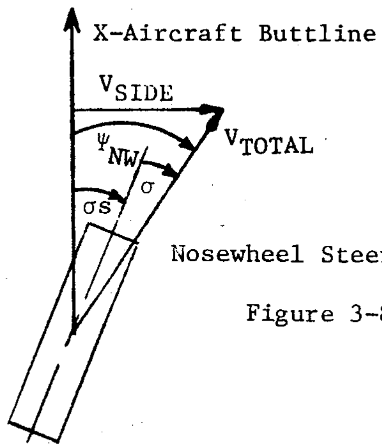

Nosewheel Steering Angle

Figure 3-8

3.3.2 Nose Wheel Steering

The nose wheel steering angle, σ_S, is commanded by the rudder pedals through a nose wheel steering actuator which has a variable rate limit as a function of side load on the turning tire.

The nose wheel steering system is represented in block diagram form as Figure 3-9.

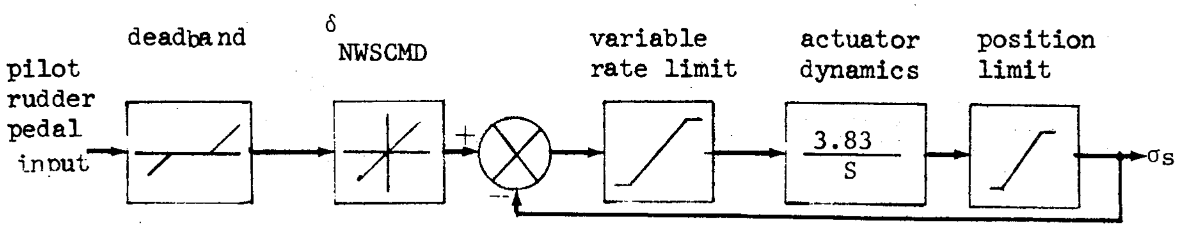

Nosewheel Steering System Block Diagram

FIGURE 3-9

In this figure:

deadband	= ± 0.1 inch of rudder travel
δ_{NWSCMD}	= the commanded nose wheel steering angle (See Figure 7-10)
variable rate limit	= 20 deg/sec no side load
	= (20 − Fy) · (.00677 deg/sec/lb) with load
actuator dynamics	= first order lag, with a time constant of .2611 seconds
position limit	= ± 13.5 (deg) from centerline

Due to the mechanical locking pin, the nose wheel strut and tire are prevented from turning until the strut has deflected a minimum of 1-1/2 inches.

3.4 BRAKING AND ANTI-SKID

The braking system is activated by the pilot applying force on the toe brakes. The pilot force applied was converted to a normalized value representing the range of no brakes to maximum braking with a dead band at zero brakes to prevent any inadvertent braking action. This is depicted in Figure 3-10.

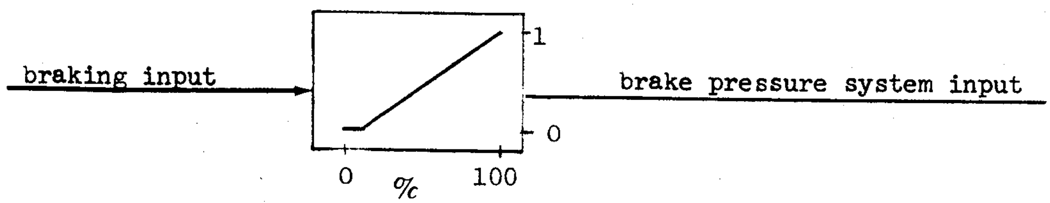

Brake Input Block Diagram

FIGURE 3-10

The amount of hydraulic pressure applied to the braking system is a function of the pilot's input and whether the anti-skid system is cycling. To represent the response of the brake pressure build up and decay, a first order lag of the form shown in Figure 3-11 was used.

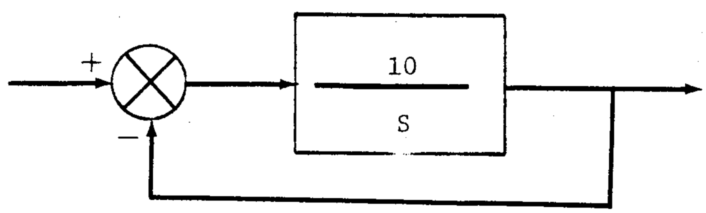

Brake Pressure Response Block Diagram

FIGURE 3-11

The anti-skid system is considered as two independent braking systems, one acting on the left main wheel and the other acting on the right main wheel, which provides the capability of differential braking. There is no braking system on the nose wheel, hence, the subscript j in the following equations of this section indicates only the left or right main wheels.

The anti-skid cycling is determined as a function of wheel velocity and the runway condition. The anti-skid cycling period is defined by the equation:

$$C_{jP} = 1.2 - 0.005 \cdot V_{jTW} \quad \text{limit } (.25 \text{ to } 1.2) \qquad (3.4\text{-}1)$$

where C_{jP} is cycle period in seconds

V_{jTW} is velocity of wheel in ft/sec

The amount of time during the cycle period that the brakes are applied is determined by equations:

dry runway-

$$C_{jT} = 1.0 - (0.001075 \cdot V_{jTW}) \qquad (3.4\text{-}2)$$

wet, flooded, or icy runway -

$$C_{jT} = 1.0 - 0.0047 \cdot V_{jTW} \text{ if } V_{jTW} \leq 85. \qquad (3.4\text{-}3)$$

$$\text{or } C_{jT} = 0.6 - 0.002941 \cdot (V_{jTW} - 85.) \text{ if } V_{jTW} > 85. \qquad (3.4\text{-}4)$$

where C_{jT} = fraction of cycle time that brakes are on.

To determine if the anti-skid system should be cycled, the commanded brake force is defined by:

$$F_{jBCOM} = A_{BRK} \cdot BK_j \cdot 3000. \qquad (3.4\text{-}5)$$

where A_{BRK} is effective braking area

BK_j is the normalized toe brake input

and 3000 PSI is the maximum hydraulic brake pressure.

The force applied at the wheel could now be calculated as

$$F_{jB} = \mu_{jB} \cdot F_{jE} \qquad (3.4\text{-}6)$$

when the brake was 'on' and

$$F_{jB} = 0 \qquad (3.4\text{-}7)$$

when the brake was 'off' during the anti-skid cycle. These equations require that the braking friction coefficient, μ_{jB}, which gives the force when the brake is on, be available as a function of surface condition and velocity or some other indicator of wheel speed. This type of data was not available since most measurements of friction coefficients are obtained from vehicle tests with the anti-skid operating. This was the case for the available data presented as μ_D in Figures 7-6 through 7-9.

Consequently, in order to simulate the anti-skid operation <u>and</u> to use the available data, it was necessary to increase the magnitude of the allowable brake force during the time that the brake was 'on' in such a manner as to insure that the total force during the cycle period was the same as indicated by the test data. This was done by first calculating the average force over the cycle period.

$$F_{jBAVG} = \mu_{jD} \cdot F_{jE} \tag{3.4-8}$$

Then, dividing this average force by the fraction of the time the brakes are 'on' during an anti-skid cycle gives the force that must act during the brake 'on' time to give the average force of equation (3.4-8).

$$F_{jBON} = F_{jBAVG}/C_{jT} \tag{3.4-9}$$

This force is the maximum force that may be permitted during the brake-'on' cycle of the anti-skid. If the commanded braking force F_{jBCOM} is less than the maximum force that can be generated between the tire and the runway, then the anti-skid would not cycle and

$$F_{jB} = F_{jBCOM} \tag{3.4-10}$$

F_{jBON} of equation (3.4-9) is then the limiting value placed on the braking force of equation (3.4-10). This limit may be realized by defining an anti-skid on/off cycle flag C_{jYC} such that

$$\begin{aligned} C_{jYC} &= 0 \text{ when } F_{jBCOM} > F_{jBON} \\ C_{jYC} &= 1 \text{ when } F_{jBCOM} \leq F_{jBON} \end{aligned} \tag{3.4-11}$$

The limiting value of F_{jB} may then be defined as

$$F_{jBMAX} = C_{jYC} \cdot F_{jBON} \tag{3.4-12}$$

which has a value of zero when the anti-skid brake is 'off' ($C_{jYC} = 0$), and a value of F_{jBON} when the anti-skid brake is 'on' ($C_{jYC} = 1$). The braking force is then determined by placing an upper limit on equation (3.4-10).

$$F_{jB} = F_{jBCOM} \Big|_{\text{Limited to } F_{jBMAX}} \tag{3.4-13}$$

Taking the braking force to act opposite to the direction of the longitudinal velocity then gives

$$F_{jGV1} = F_{jB} \tag{3.4-14}$$

3.5 STRUT DYNAMICS

The previous sections have defined the generation of the components of a force vector $\overline{F}_V$ aligned in a gear velocity axis system. Equation (3.1-6) indicates the transformation of these forces to axis systems aligned with each gear. Neglecting the forces that would cause bending in the gear, leaves only the component F_{jG3} to consider in the development of the strut dynamic relations.

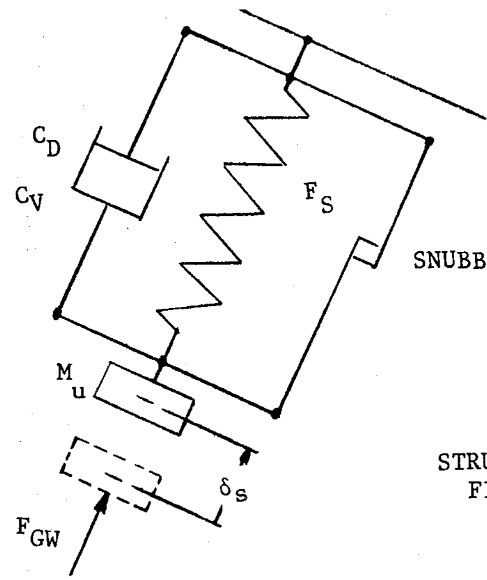

STRUT DYNAMIC MODEL
FIGURE 3-12

The strut dynamics may be derived by considering the strut as a spring, mass, damper system. However, neither the spring nor the damper are considered to be linear. The force in the spring F_{jS} is calculated from the load-stroke curve of Figure 7-1 for the nose strut and Figure 7-2 for the main gear struts.

The damper is assumed to have a linear viscous component F_{jD} and a component proportional to the square of the compression rate (velocity squared damping) F_{jV}. The linear damping coefficient is a constant, C_{Di}. The velocity squared coefficient C_{Vj} is a function of deflection, Tables 7-2 and 7-3, and is much greater for an opening damper than it is for a closing damper.

$$F_{jD} = C_{Di}\,\dot{\delta}_{js} \tag{3.5-1}$$

$$F_{jV} = C_{Vj}\,|\dot{\delta}_{js}|\,\dot{\delta}_{js} \tag{3.5-2}$$

The total damping force is then

$$F_{jDAMP} = F_{jD} + F_{jV} \tag{3.5-3}$$

Noting that

$$F_{jGW} = -F_{jG3} \tag{3.5-4}$$

summing the forces acting on the unsprung mass gives

$$F_{jGW} - F_{jDAMP} - F_{jS} = m_{uj}\ddot{\delta}_{jS} \tag{3.5-5}$$

or
$$\ddot{\delta}_{jS} = \frac{F_{jGW} - F_{jDAMP} - F_{jS}}{m_{u_j}} \tag{3.5-6}$$

where equation (3.5-6) is equivalent to (3.1-7).

Two limits are placed on the above relations. First is the snubber which limits δ_{js} to positive values only. The second is a limit placed on the total damping force F_{jDAMP}. This limit restricts the magnitude of the damping force such that a motion reversal cannot occur until the magnitude of the force in the spring F_{jS} has reached a value equal and opposite, to the ground force F_{jGW}. When $\dot{\delta}_{js} > 0$ (compressing strut) and $(F_{jGW} - F_{jS}) > 0$, then F_{jDAMP} is limited to a maximum value of $F_{jGW}-F_{jS}$. When $\dot{\delta}_{js} < 0$ (extending strut), and $(F_{jGW}-F_{jS}) < 0$, then F_{jDAMP} is limited to a minimum value of $(F_{jGW}-F_{jS})$.

4.0 RUNWAY MODEL

A runway model is considered to have certain roughness characteristics and a slope from the center to the edge representing a runway crown. The runway model also contains varying friction characteristics representing different weather conditions. These friction characteristics are considered to either be constant over the entire runway surface or to vary between patches of the runway.

4.1 RUNWAY CROWN AND ROUGHNESS

To establish the height of the crown or the height of the roughness bump at each wheel, it is first necessary to locate the wheel with respect to some runway reference point. For this development, the far end of the runway at the runway centerline is taken as the reference point (EOR). Both the latitude (Γ_{RWY}) and longitude (Ω_{RWY}) of this reference point are known quantities. At any given time, the latitude (Γ_{cg}) and longitude (Ω_{cg}) of the aircraft's center-of-gravity are also known quantities determined from the solution of the aircraft's equations-of-motion (EOM). The vector components in aircraft body axes of the vector $\overline{R}_j$ which locates the j^{th} wheel with respect to the aircraft's c.g. are also known from equation (6.1-4) developed later.

Figure 4-1 represents the geometrical relations

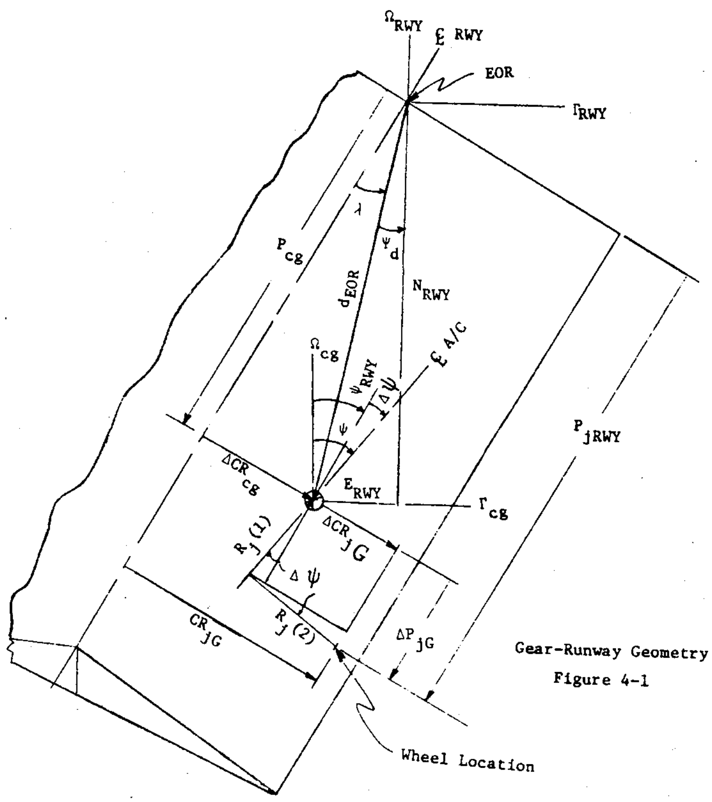

Gear-Runway Geometry
Figure 4-1

between the aircraft's c.g. and wheel locations and the end of the runway reference point. The parameter N_{RWY} represents the distance North from the aircraft's c.g. to the EOR reference point and E_{RWY} represents the distance East from the c.g. to the EOR. These are determined from the differences in latitude and longitude respectively.

$$N_{RWY} = (\Gamma_{RWY} - \Gamma_{cg}) \cdot C_{DLTF} \tag{4.1-1}$$

$$E_{RWY} = (\Omega_{RWY} - \Omega_{c.g.}) \cdot C_{DLNF} \tag{4.1-2}$$

where C_{DLTF} is the constant conversion factor converting degrees latitude to feet, and C_{DLNF} converts degrees longitude to feet and is a function of the runway latitude. The direct distance from the c.g. to the EOR reference point may then be calculated from:

$$d_{EOR} = (N^2_{RWY} + E^2_{RWY})^{\frac{1}{2}} \tag{4.1-3}$$

and the heading of this direct distance line is given by:

$$\Psi_d = \tan^{-1}(E_{RWY}/N_{RWY}) \tag{4.1-4}$$

The position of the c.g. from the EOR along the runway centerline (P_{cg}) is then determined by first calculating an auxilliary angle λ as

$$\lambda = \psi_{RWY} - \Psi_d \tag{4.1-5}$$

and then using this angle to calculate

$$P_{cg} = d_{EOR} \cos \lambda \tag{4.1-6}$$

The distance across the runway from the centerline to the c.g. is then

$$\Delta CR_{cg} = d_{EOR} \sin \lambda \tag{4.1-7}$$

The location of the j^{th} wheel on the runway is then determined by adding the contributions of the location of the wheel with respect to the c.g. The cross runway contribution is determined by first defining the angle $\Delta\psi$ as the difference between the runway heading ψ_{RWY} and the direction the fuselage is pointing ψ.

$$\Delta\psi = \psi - \psi_{RWY} \tag{4.1-8}$$

Then

$$\Delta CR_{jG} = R_j\ (1) \sin \Delta\psi + R_j\ (2) \cos \Delta\psi \tag{4.1-9}$$

where it is noted that the vector component R_j (1) is negative for both main wheels and positive for the nose wheel. Also, R_j (2) is negative for the left main wheel, positive for the right main wheel and zero for the nose wheel.

The distance along the runway from the c.g. to the j^{th} wheel is then determined as

$$\Delta P_{jg} = R_j(2) \sin \Delta\psi - R_j(1) \cos \Delta\psi \qquad (4.1\text{-}10)$$

The cross runway distance from the runway centerline to the wheel is then the sum of terms from equations (4.1-7) and (4.1-9).

$$CR_{jg} = \Delta CR_{cg} + \Delta CR_{jg} \qquad (4.1\text{-}11)$$

Similarly the position of the j^{th} wheel along the runway from the EOR point is the sum of terms from equations (4.1-6) and (4.1-10).

$$P_{jRWY} = P_{cg} + \Delta P_{jG} \qquad (4.1\text{-}12)$$

The crown of the runway is assumed to be of uniform slope RW_s from the maximum thickness at the centerline to zero thickness at the edge. Defining the width of the runway as RW_W, the height of the runway at the centerline is

$$h_{R℄} = \frac{1}{2} RW_W \cdot RW_s \qquad (4.1\text{-}13)$$

The height of the runway due to the crown at the j^{th} wheel location may then be calculated as

$$h_{jCRN} = h_{R℄} - |CR_{jg}| \cdot RW_s \qquad (4.1\text{-}14)$$

The runway roughness profile was taken from a 2400 foot section of Travis A.F.B. This data is presented in Table 7-1 of Section 7.0. Normally, the total runway length to be used will be greater than the section of roughness data available. Defining ℓ_{RGH} as the length of the section of roughness data and L_{RWY} as the the length of the runway where

$$L_{RWY} > \ell_{RGH} \qquad (4.1\text{-}15)$$

it is necessary to repeat the roughness pattern several times over the length of the runway. Hence, it is necessary to determine the location of each wheel within the roughness sector. This may be done by defining the number of sectors between the wheel location and the end of the runway as

$$P_{jN} = P_{jRWY}/\ell_{RGH} \qquad (4.1\text{-}16)$$

Then defining the integer portion of this number as I_{jRWY}, the position of the wheel within the sector may be determined by

$$P_{jRGH} = (P_{jN} - I_{jRWY}) \cdot \ell_{RGH} \qquad (4.1\text{-}17)$$

The height of the runway due to roughness at each gear location, h_{jBMP}, may then be obtained from Table 7-1 as a functional relation of P_{jRGH}

$$h_{jBMP} = f(P_{jRGH})\Big|_{TABLE\ 7-1} \qquad (4.1\text{-}18)$$

The total height of the runway surface above ground level at each wheel is then the sum of the height of the crown from equation (4.1-14) with the height of the bump from equation (4.1-18).

$$h_{jRWY} = h_{jCRN} + h_{jBMP} \qquad (4.1\text{-}19)$$

4.2 RUNWAY CONDITION PROFILES

To evaluate the ground handling characteristics of the airplane with the four different types of runway surface conditions of dry, wet, flooded, or icy; the program was structured such that any one of the four conditions could be selected. In addition to the four runway conditions fixed for the entire length of the runway, four cases of patchy runway condition profiles were available. These profiles varied the runway conditions as a function of the distance down the runway from the threshold. These four cases are presented in Figure 7-3. The equations to determine the distance from the threshold for each gear are similar to those used to determine gear position for use in the runway roughness profile calculations. For the patchy runway profiles, the runway condition at each wheel may be different.

The different runway conditions influence the determination of the proper braking and side force friction coefficient curves to use for each wheel. For each of the four runway conditions, there is an associated side force coefficient curve. For the main gear there is an additional set of side force coefficient curves depending on whether or not the anti-skid braking system is cycling.

The main gear also have a set of braking friction coefficient curves which are utilized depending on which of the four runway conditions exist at the wheel. The nose gear has no braking capability.

All of these coefficient curves are a function of the wheel velocity and the skid angle of the tire. The skid angle is defined in section 3.3.1. These side force, μ_{jS}, and braking, μ_{jD}, coefficient curves are presented in Figures 7-4 thru 7-9. These coefficients are multiplied by the normal force acting on the wheel in question to obtain the side and aft forces due to friction acting at the wheel.

$$F_{jY} = \mu_{jS} \cdot F_{jE} \tag{4.2-1}$$

$$F_{jB} = \mu_{jD} \cdot F_{jE} \tag{4.2-2}$$

As shown in equations (3.2-5), (3.3-1), and (3.4-14), these relations are used to establish the force vector $\overline{F}_{jGV}$ at each wheel. The technique for determining the braking force F_{jB} more exactly is described in Section 3.3 when an anti-skid system is included.

$$\overline{F}_{jGV} = \begin{Bmatrix} F_{jGV1} \\ F_{jGV2} \\ F_{jGV3} \end{Bmatrix} = \begin{Bmatrix} -F_{jB} \\ -F_{jY} \cdot SSK_j \\ -F_{jE} \end{Bmatrix} \tag{4.2-3}$$

5.0 TRANSFORMATIONS AND AXIS SYSTEMS

Several of the force and velocity vectors must be transformed from one axis system to another in order to utilize them properly in the LNDGR subroutine. Basically, the transformation of a vector from one system to another takes the form

$$\bar{V} = B^T A \quad \bar{X} \qquad (5.0\text{-}1)$$

where: $\bar{V}$ is a three component vector in the new axis system B;

$$\bar{V} = \left.\begin{matrix} V_1 \\ V_2 \\ V_3 \end{matrix}\right\} \qquad (5.0\text{-}2)$$

$\bar{X}$ is a three component vector in the old axis system A;

$$\bar{X} = \left.\begin{matrix} X_1 \\ X_2 \\ X_3 \end{matrix}\right\} \qquad (5.0\text{-}3)$$

and $B^T A$ is a 3 X 3 transformation matrix between the old system A and the new axis system B;

$$B^T A = \begin{bmatrix} C_{11} & C_{12} & C_{13} \\ C_{21} & C_{22} & C_{23} \\ C_{31} & C_{32} & C_{33} \end{bmatrix} \qquad (5.0\text{-}4)$$

This section defines the different axis systems used in the LNDGR subroutine and develops the basic transformations between the different systems. The matrix subscript notation is used to reflect the reverse order of transformation:

$B^T A$ transforms a vector from system A to system B;

$A^T B$ transforms a vector from system B to system A;

of course

$$A^T B \;=\; B^T A^{\,-1} \qquad (5.0\text{-}5)$$

where the -1 superscript indicates the inverse of a matrix.

This reverse order subscripting is used as a bookkeeping aid when performing matrix multiplications to develop new transformations. In other words, a transformation from axis system A to axis system C may be expressed

$$C^T A = C^T B \; B^T A \tag{5.0-6}$$

given that the transformations from A to an intermediate system B and from B to the desired system C are known. This indicates that a vector is first transformed from system A to system B by $B^T A$; the vector in system B is then transformed to system C by $C^T B$.

5.1 AXIS SYSTEM DEFINITIONS

All axis systems used are made of three orthogonal axes that follow the right hand rotation rules demonstrated in Figure 5-1.

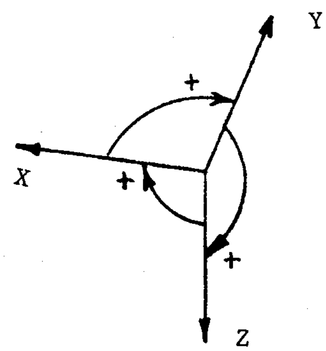

Right Hand Rotation
Figure 5-1

5.1.1 Local Vertical Axis System

The Local Vertical (LV) axis system is defined by locating an axis down along the gravity vector toward the center of the Earth. The other two axes are located in a plane normal to the down axis. These two axes are oriented such that one points North and the other East as shown in Figure 5-2. Hence, this system is sometimes referred to as a North, East, Down (N.E.D.) system.

Local Vertical Axes
Figure 5-2

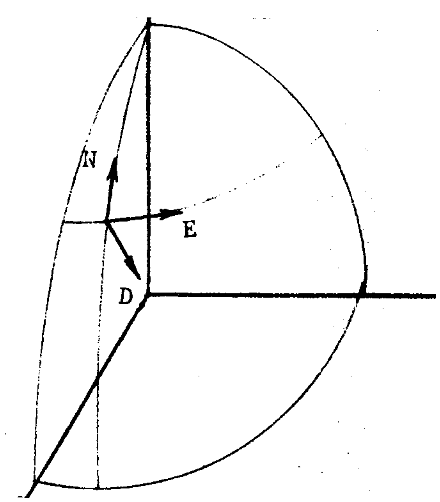

5.1.2 Horizontal Axis System

This axis system also has one axis located down along the gravity vector toward the center of the Earth. The other two axes are orthogonal and lie in the horizontal plane; however, one is located along the projection of the aircraft's longitudinal axis on the horizontal plane and the other in the direction of the aircraft's right wing.

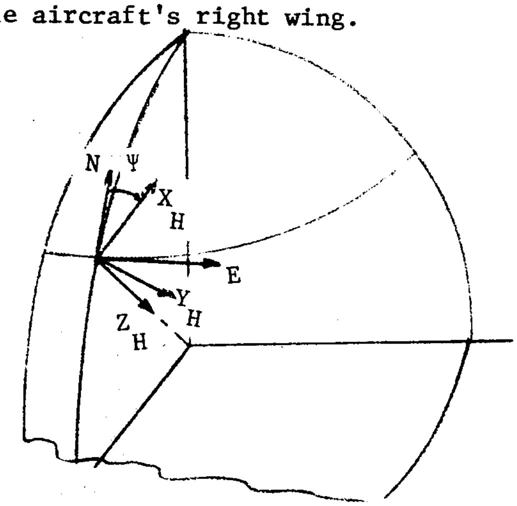

HORIZONTAL AXIS SYSTEM
Figure 5-3

The angle between the North axis and the X axis of this system is the Euler angle ψ . This system is shown in Figure 5-3.

5.1.3 Aircraft Body Axis System

This system is defined with the X-axis along the fuselage center line, positive forward. The Y-axis lies in the center plane of the aircraft, positive in the direction of the right wing and intersects the X-axis at the center of gravity of the aircraft. The Z-axis is then normal to the X-Y plane and positive through the bottom of the fuselage as depicted in Figure 5-4.

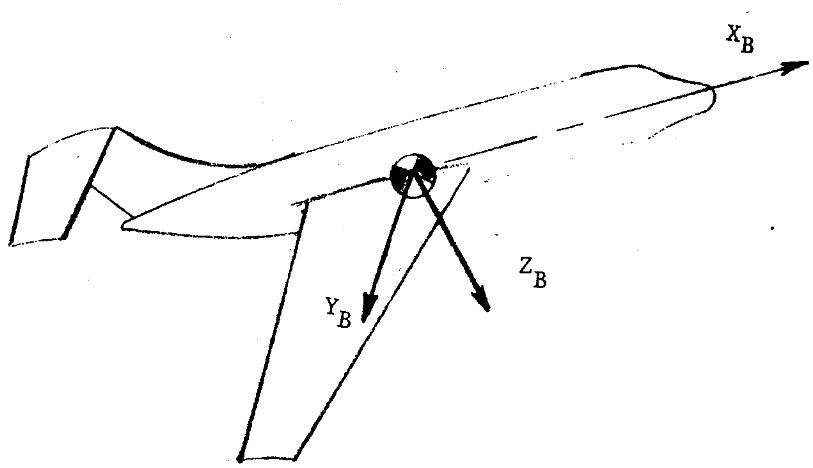

BODY AXIS SYSTEM
Figure 5-4

5.1.4 Gear Velocity Axis Systems

The GEAR velocity axis systems are defined at each wheel. As shown in Figure 5-5, the X-axis is defined to lie along the component of the local velocity at the wheel in the horizontal plane. The Y-axis is in the horizontal plane and positive to the right of the aircraft. The Z-axis is down, normal to the horizontal plane.

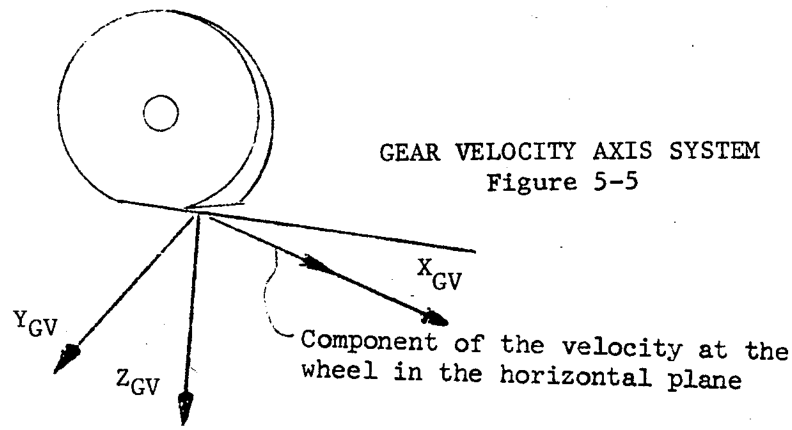

GEAR VELOCITY AXIS SYSTEM
Figure 5-5

5.1.5 Landing Gear Axis Systems

The Z-axes of the Landing Gear axis systems are defined as positive down along the gear struts. The X and Y axes are then orthogonal to the struts with the X axis positive forward and the Y axis positive toward the right side of the aircraft. This system is described pictorially in Figure 5-6.

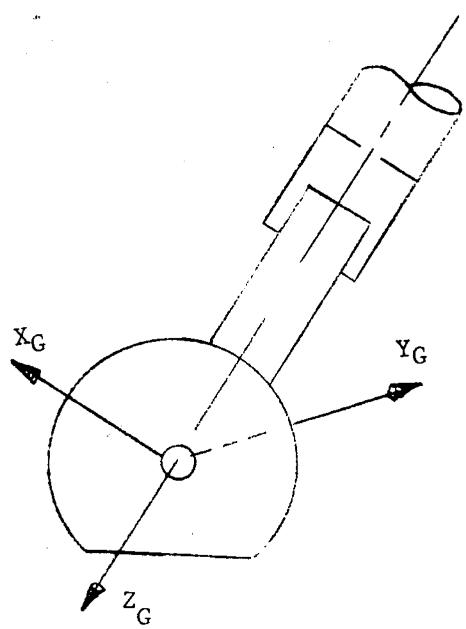

LANDING GEAR AXIS SYSTEM
Figure 5-6

5.2 TRANSFORMATIONS

The transform matrices used in the program are all derived by considering single angle rotations between one system and the next. Matrix multiplication is then used to arrive at the matrices for transforms involving more than one angular rotation.

5.2.1 Local Vertical to Horizontal

As depicted in the discussion of Section 5.1.2, the X-axis of the Horizontal Axis system is offset from the North axis of the local vertical axis system by the Euler angle ψ.

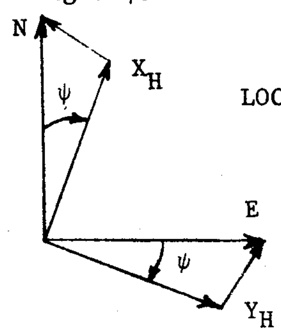

LOCAL VERTICAL TO HORIZONTAL TRANSFORMATION
Figure 5-7

The angle ψ is achieved by rotating the NED system about the D axis which is also the Z axis of the horizontal system. Closing the vector triangles as shown in Figure 5-7, the components in the horizontal system may be expressed in terms of the components in the local vertical system as:

$$\begin{aligned} X_H &= N \cos \psi + E \sin \psi \\ Y_H &= -N \sin \psi + E \cos \psi \\ Z_H &= D \end{aligned} \qquad (5.2\text{-}1)$$

Writing these expressions in Matrix form gives the transformation matrix transforming a vector in the local vertical system in to a vector in the horizontal system.

$$\left.\begin{matrix} X_H \\ Y_H \\ Z_H \end{matrix}\right\} = \begin{bmatrix} \cos\psi & \sin\psi & 0 \\ -\sin\psi & \cos\psi & 0 \\ 0 & 0 & 1 \end{bmatrix} \cdot \left\{\begin{matrix} N \\ E \\ D \end{matrix}\right\} \tag{5.2-2}$$

or

$$\overline{X}_H = {}_H T_{LV} \cdot \overline{N} \tag{5.2-3}$$

where

$${}_H T_{LV} = \begin{bmatrix} \cos\psi & \sin\psi & 0 \\ -\sin\psi & \cos\psi & 0 \\ 0 & 0 & 1 \end{bmatrix} \tag{5.2-4}$$

5.2.2 Horizontal to Aircraft Body

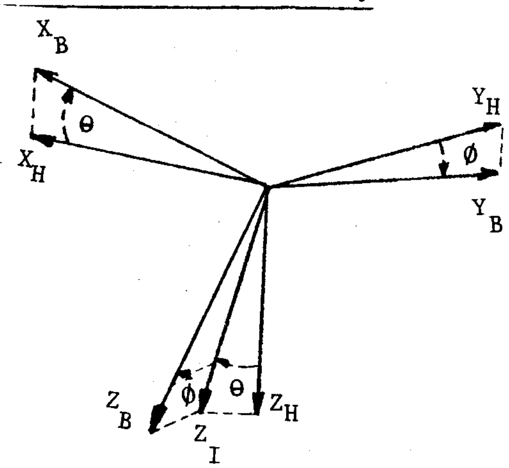

HORIZONTAL TO AIRCRAFT BODY TRANSFORMATION
Figure 5-8

The transformation between the horizontal and the aircraft body axes systems involves a combination of two single angle transformations as described in Figure 5-8. First, a transformation is made between the horizontal system and an intermediate system through the Euler pitch angle θ. Then a transformation is made through the Euler roll angle ϕ from the intermediate system to the final body axis system.

Considering first the transformation from the horizontal system to the intermediate axes through the pitch angle θ, a rotation about the horizontal lateral axis Y_H, positive nose up gives the Euler angle θ.

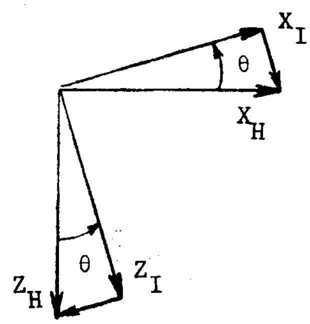

$$
\begin{aligned}
X_I &= X_H \cos\theta - Z_H \sin\theta \\
Y_I &= Y_H \qquad\qquad (5.2\text{-}5) \\
Z_I &= X_H \sin\theta + Z_H \cos\theta
\end{aligned}
$$

In transform form we have

$$\overline{X}_I = {}_I T_H \cdot \overline{X}_H \qquad (5.2\text{-}6)$$

where

$${}_I T_H = \begin{bmatrix} \cos\theta & 0 & -\sin\theta \\ 0 & 1 & 0 \\ \sin 0 & 0 & \cos\theta \end{bmatrix} \qquad (5.2\text{-}7)$$

Next, the transformation from the intermediate axes system to the aircraft body axis system is determined through a rotation about the intermediate longitudinal axis X_I. This rotation results in an angle ϕ, defined as positive with the right wing down.

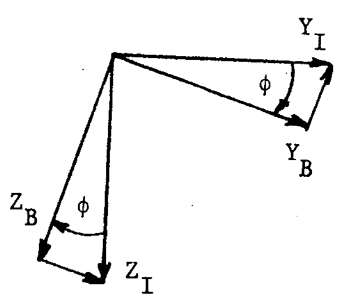

$$
\begin{aligned}
X_B &= X_I \\
Y_B &= Y_I \cos\phi + Z_I \sin\phi \qquad (5.2\text{-}8) \\
Z_B &= -Y_I \sin\phi + Z_I \cos\phi
\end{aligned}
$$

Writing the transform relation

$$\overline{X}_B = {}_B T_I \cdot \overline{X}_I \tag{5.2-9}$$

where from (5.2-8) the transformation is defined

$${}_B T_I = \begin{bmatrix} 1 & 0 & 0 \\ 0 & \cos\phi & \sin\phi \\ 0 & -\sin\phi & \cos\phi \end{bmatrix} \tag{5.2-10}$$

The complete transformation from the horizontal to the body axis system may be developed from relations (5.2-6) and 5.2-9).

$$\overline{X}_B = {}_B T_I \; {}_I T_H \; \overline{X}_H \tag{5.2-11}$$

or

$$\overline{X}_B = {}_B T_H \; \overline{X}_H \tag{5.2-12}$$

where

$${}_B T_H = {}_B T_I \; {}_I T_H \tag{5.2-13}$$

Substituting (5.2-10) and (5.2-7) into (5.2-13 gives

$${}_B T_H = \begin{bmatrix} 1 & 0 & 0 \\ 0 & \cos\phi & \sin\phi \\ 0 & -\sin\phi & \cos\phi \end{bmatrix} \begin{bmatrix} \cos\theta & 0 & -\sin\theta \\ 0 & 1 & 0 \\ \sin\theta & 0 & \cos\theta \end{bmatrix}$$

Introducing the notation $C\phi = \cos\phi$, $S\phi = \sin\phi$, $C\theta = \cos\theta$ and $S\theta = \sin\theta$ and performing the indicated matrix multiplication yields the transformation matrix required to transform from the horizontal axis system to the aircraft body axis system.

$${}_B T_H = \begin{bmatrix} C\theta & 0 & -S\theta \\ S\phi S\theta & C\phi & S\phi C\theta \\ C\phi S\theta & -S\phi & C\phi C\theta \end{bmatrix} \tag{5.2-14}$$

5.2.3 Local Vertical to Aircraft Body

The transformation matrices required to transform directly from the local vertical (NED) axis system to the aircraft body axis system are available in the previous developments. Combining equations (5.2-3) and (5.2-12) gives

$$\overline{X}_B = B^T{}_H \cdot H^T{}_{LV} \cdot \overline{N} \tag{5.2-15}$$

or

$$\overline{X}_B = B^T{}_{LV}\ \overline{N} \tag{5.2-16}$$

where

$$B^T{}_{LV} = B^T{}_H \cdot H^T{}_{LV} \tag{5.2-17}$$

Substituting from (5.2-4) and (5.2-14) into (5.2-17) gives

$$B^T{}_{LV} = \begin{bmatrix} C\theta & 0 & -S\theta \\ S\phi S\theta & C\phi & S\phi C\theta \\ C\phi S\theta & -S\phi & C\phi C\theta \end{bmatrix} \begin{bmatrix} \cos\psi & \sin\psi & 0 \\ -\sin\psi & \cos\psi & 0 \\ 0 & 0 & 1 \end{bmatrix} \tag{5.2-18}$$

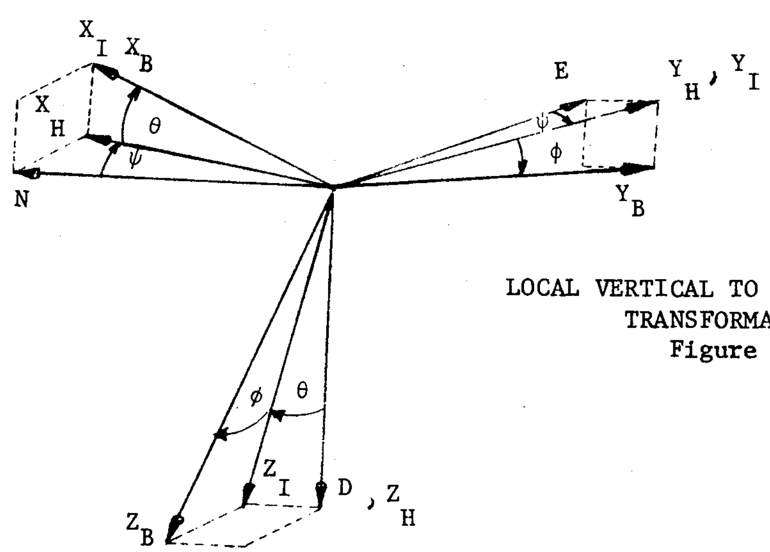

LOCAL VERTICAL TO AIRCRAFT BODY TRANSFORMATION
Figure 5-9

Using $C\psi$ for cos ψ and $S\psi$ for sin ψ and performing the matrix multiplication gives the final three angle transformation:

$$
{}_B T_{LV} = \begin{bmatrix} C\theta C\psi & C\theta S\psi & -S\theta \\ (S\phi S\theta C\psi - C\phi S\psi) & (S\phi S\theta S\psi + C\phi C\psi) & S\phi\ C\theta \\ (C\phi S\theta C\psi + S\phi S\psi) & (C\phi S\theta S\psi - S\phi C\psi\ ) & C\phi\ C\theta \end{bmatrix}
$$

The angles and axes used in this transformation are shown in Figure 5-9.

5.2.4 Gear to Aircraft Body

When a landing gear is in its normal extended position, the centerline of the strut is not necessarily perpendicular to the waterline planes of the aircraft. Figure 5-10 demonstrates that two angles may be used to define the relationship between the strut centerline - which is seen from Section 5.1.5 to be the Z-axis of the landing gear axis system - and the aircraft. The first is the angle P_{iG} which is the angle between the aircraft stationline (aircraft body Y-Z plane) and the strut centerline.

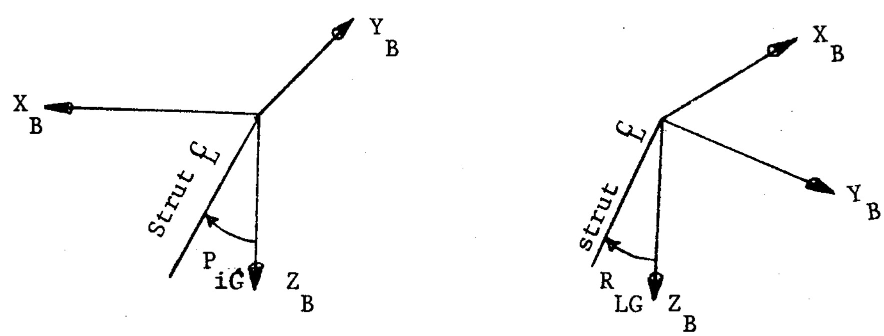

STRUT ANGLE RELATIONS
Figure 5-10

This angle is defined as positive for a forward rotation of the strut and is applicable to both main and nose gears. The second angle is R_{LG} which is the angle between the buttline (aircraft body X-Z plane) and the strut centerline. This angle is defined as positive for the left gear strut extending outboard from the X-Z plane. The nose gear equivalent of this angle is zero and the right gear angle is the negative of the left gear angle.

With these angular definitions, the Euler angle rotational method cannot be used directly to determine the transformations. An intermediate relation between one of these angles and a related Euler angle must first be defined. Consider Figure 5-11.

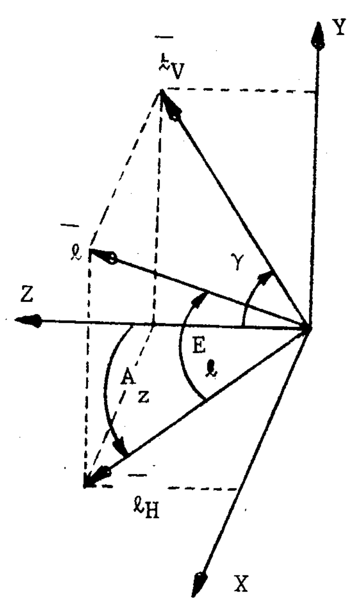

VECTOR PROJECTION
Figure 5-11

The vector $\overline{\ell}$ has components x,y,z along the X,Y,Z axes respectively. The vector $\overline{\ell}$ also has projections $\overline{\ell}_H$ in the X-Z plane and $\overline{\ell}_v$ in the Y-Z plane. The component $\overline{\ell}_v$ makes an angle γ with the Z-axis in the Y-Z plane. Trigonometric relations may be used to express the components in terms of each other.

$$\begin{aligned} \overline{\ell}_H &= \overline{\ell} \cos E\ell \\ y &= \overline{\ell} \sin E\ell \\ z &= \overline{\ell}_V \cos \gamma \\ y &= \overline{\ell}_V \sin \gamma \\ z & \overline{\ell}_H \cos A_z \\ x &= \overline{\ell}_H \sin A_z \end{aligned} \tag{5.2-20}$$

Equating the two expressions for y

$$y = \overline{\ell} \sin E_\ell = \overline{\ell}_v \tag{5.2-21}$$

Then from the two expressions for z

$$z = \overline{\ell}_V \cos \gamma = \overline{\ell}_H \cos A_z$$

or

$$\overline{\ell}_V = \overline{\ell}_H \cdot \frac{\cos A_z}{\cos \gamma} \tag{5.2-22}$$

and substituting for the expression for $\overline{\ell}_H$

$$\overline{\ell}_V = \overline{\ell} \cos E_\ell \cdot \frac{\cos A_z}{\cos \gamma} \tag{5.2-23}$$

Then putting this $\overline{\ell}_v$ into the y equality (5.2-21)

$$\overline{\ell} \sin E\ell = \overline{\ell} \cos E_\ell \cdot \cos A_z \; \frac{\sin \gamma}{\cos \gamma}$$

which reduces to

$$\tan E_\ell = \tan \gamma \cos A_z \tag{5.2-24}$$

Now, note that the angles A_z and E_ℓ as used here are Euler type angles. The angle γ is not. However, it is also noted that the angle γ may be associated with the angle R_{LG} in the Y_B-Z_B plane and the angle A_z may be associated with the angle P_{jG} in the X_B-Z_B plane which are used to express the angular relations between the strut centerline and the aircraft. Hence, we may define an auxillary Euler angle A_{jEA} and use it to determine the transform relations between the Gear axis system and the Aircraft Body axis system.

Relating to equation (5.2-24)

$$\tan A_{jEA} = \tan R_{jG} \cos P_{jG} \qquad (5.2\text{-}25)$$

The rotation relations for the transformation may then be developed. Rotating about the Y_B axis through the angle P_{iG} to the intermediate axis system.

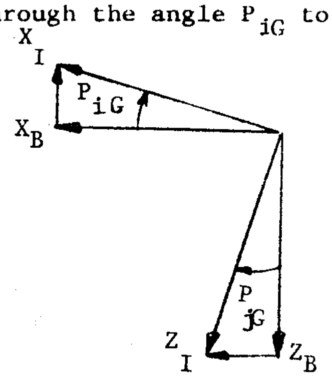

$$X_B = X_I \cos P_{iG} + Z_I \sin P_{iG}$$

$$Y_B = Y_I \qquad (5.2\text{-}26)$$

$$Z_B = -X_I \sin P_{iG} + Z_I \cos P_{iG}$$

or $\overline{X}_B = {}_B T_I \cdot \overline{X}_I$ (5.2-27)

where

$${}_B T_I = \begin{bmatrix} \cos P_{iG} & 0 & \sin P_{iG} \\ 0 & 1 & 0 \\ -\sin P_{iG} & 0 & \cos P_{iG} \end{bmatrix} \qquad (5.2\text{-}28)$$

Then rotating about X_I through the auxiliary angle A_{jEA}

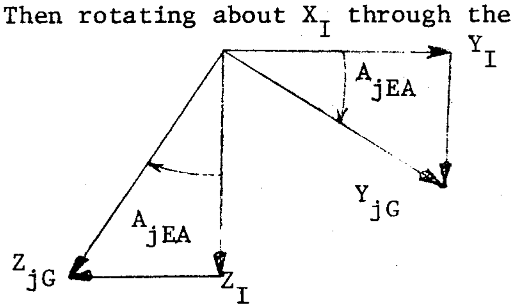

$$X_I = X_{jG} \qquad (5.2\text{-}29)$$

$$Y_I = Y_{jG} \cos A_{jEA} - Z_{jG} \sin A_{jEA}$$

$$Z_I = Y_{jG} \sin A_{jEA} + Z_{jG} \cos A_{jEA}$$

Or $\overline{X}_I = {}_I T_{jG} \cdot \overline{X}_{jG}$ (5.2-30)

where

$${}_I T_{jG} = \begin{bmatrix} 1 & 0 & 0 \\ 0 & \cos A_{jEA} & -\sin A_{jEA} \\ 0 & \sin A_{jEA} & \cos A_{jEA} \end{bmatrix} \qquad (5.2\text{-}31)$$

The total transform from gear to body may then be written.

$$\overline{X}_B = {}_B T_I \cdot {}_I T_{jG} \cdot \overline{X}_{jG} = {}_B T_{jG} \cdot \overline{X}_{jG} \qquad (5.2\text{-}32)$$

Where:

$${}_B T_{jG} = {}_B T_I \cdot {}_I T_{jG} = \begin{bmatrix} \cos P_{iG} & 0 & \sin P_{iG} \\ 0 & 1 & 0 \\ -\sin P_{iG} & 0 & \cos P_{iG} \end{bmatrix} \begin{bmatrix} 1 & 0 & 0 \\ 0 & \cos A_{EA} & -\sin A_{EA} \\ 0 & \sin A_{EA} & \cos A_{EA} \end{bmatrix}$$

and performing the matrix multiplication gives

$${}_B T_{iG} = \begin{bmatrix} \cos P_{iG} & \sin P_{iG} \sin A_{jEA} & \sin P_{iG} \cos A_{jEA} \\ 0 & \cos A_{jEA} & -\sin A_{jEA} \\ -\sin P_{iG} & \cos P_{iG} \sin A_{jEA} & \cos P_{iG} \cos A_{jEA} \end{bmatrix} \qquad (5.2\text{-}33)$$

Now look at expression (5.2-25), in a digital routine it is necessary to perform the multiplication and then take the arctangent to obtain the angle A_{jEA} for use in the transformation expression (5.2-33).

$$A_{jEA} = \text{Tan}^{-1} (\text{Tan } R_{jG} \cos P_{iG}) \qquad (5.2\text{-}34)$$

However, it should be noted that as long as P_{iG} is in the neighborhood of 10° or less, $\cos P_{iG} \approx .99$. Hence, the Euler angle A_{jEA} may be approximated directly by R_{jG}; thus saving the compute time required for the arctangent calculation.

$$A_{jEA} \approx R_{jG} \quad \text{when } P_{iG} \leq 10° \qquad (5.2\text{-}35)$$

Also, it is again noted that the angle R_{jG} is zero for the nose gear. Hence the transformation from nose gear to aircraft body axis system is given by equation (5.2-28)

$${}_B T_{NG} = \begin{bmatrix} \cos P_{NG} & 0 & \sin P_{NG} \\ 0 & 1 & 0 \\ -\sin P_{NG} & 0 & \cos P_{NG} \end{bmatrix} \qquad (5.2\text{-}36)$$

The transformation from the left main gear to aircraft body axes is obtained by substituting P_{LG} for P_{iG} and R_{LG} for A_{jEA} in (5.2-33). The transform from the right main gear to aircraft body axes is obtained by substituting $R_{jG} = -R_{LG}$ in the transform development. Using the approximation (5.2-35) with (5.2-33) and (5.2-37), this becomes:

$$
{}_{B}{}^{T}{}_{RG} = \begin{bmatrix} \cos P_{RG} & -\sin P_{RG} \sin R_{LG} & \sin P_{RG} \cos R_{LG} \\ 0 & \cos R_{LG} & \sin R_{LG} \\ \sin P_{RG} & -\cos P_{RG} \sin R_{LG} & \cos P_{RG} \cos R_{LG} \end{bmatrix} \quad (5.2\text{-}38)
$$

5.2.5 <u>Gear Velocity to Horizontal</u>

The Gear Velocity axis system is defined with the X-axis in the horizontal plane and aligned with the total velocity component at the wheel as described in section 4.1.4. The horizontal axis system is defined with its X-axis also in the horizontal plane and aligned with the projection of the aircraft's longitudinal axis in the horizontal plane. Defining the angle between the velocity vector at the j^{th} wheel and the projected longitudinal axis of the aircraft's body X_H as Ψ_{jW}, the transform relations may be developed.

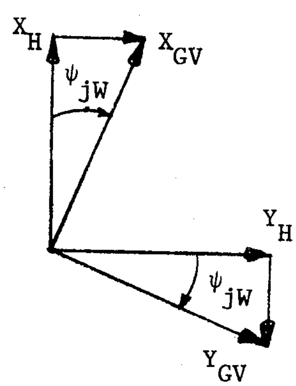

(5.2-39)

$$X_H = X_{jGV} \cos\Psi_{jW} - Y_{jGV} \sin\Psi_{jW}$$

$$Y_H = X_{jGV} \sin\Psi_{jW} + Y_{jGV} \cos\Psi_{jW}$$

$$Z_H = Z_{jGV}$$

or $\quad \overline{X}_H = H^T{}_{jGV} \cdot \overline{X}_{jGV} \quad$ (5.2-40)

where

$$
H^T{}_{jGV} = \begin{bmatrix} \cos \psi_{jW} & -\sin \psi_{jW} & 0 \\ \sin \psi_{jW} & \cos \psi_{jW} & 0 \\ 0 & 0 & 0 \end{bmatrix} \quad (5.2\text{-}41)
$$

The angles Ψ_{LW} and Ψ_{RW} are equivalent to the skid angle of equation (3.3-2). The angle Ψ_{NW} is defined by equation (3.3-5)

5.2.6 Horizontal To Gear

The transformations from the Horizontal axis system to the three gear axis systems may be obtained from relations developed in Sections 5.2.2 and 5.2.4. Denoting the transformation from the jth gear to the aircraft body axes as ${}_B T_{jG}$, the transformation from the aircraft body to the jth gear axes is the inverse relation

$$ {}_{jG}T_B = {}_B T_{jG}^{-1} \tag{5.2-42}$$

The transformation to the jth gear from the Horizontal axis system may then be written

$$ {}_{jG}T_H = {}_{jG}T_B \cdot {}_B T_H \tag{5.2-43}$$

where ${}_B T_H$ is determined from equation (5.2-14), and equations (5.2-33), (5.2-38), and (5.2-36) are used in expression (5.2-42) to obtain ${}_{MG}T_B$ and ${}_{NG}T_B$ respectively. To illustrate, the transformation ${}_{NG}T_B$ is obtained from (5.2-36) in (5.2-42) as

$$ {}_{NG}T_B = \begin{bmatrix} \cos P_{NG} & 0 & -\sin P_{NG} \\ 0 & 1 & 0 \\ \sin P_{NG} & 0 & \cos P_{NG} \end{bmatrix} \tag{5.2-44}$$

and it is noted that for transformation matrices involving Euler angles, the inverse is simply the transpose obtained by interchanging rows and columns. Equations (5.2-44) with (5.2-14) into (5.2-43) then yields the desired transformation ${}_{NG}T_H$.

$$ {}_{NG}T_H = \begin{bmatrix} \cos P_{NG} C\theta - \sin P_{NG} C\phi \; S\theta & \sin P_{NG} S\phi & -\cos P_{NG} \; S\theta \; -\sin P_{NG} C\theta \; C\phi \\ S\phi \; S\theta & C\phi & S\phi \; C\theta \\ \sin P_{NG} C\theta + \cos P_{NG} C\phi \; S\theta & -\cos P_{NG} S\phi & -\sin P_{NG} S\theta + \cos P_{NG} C\theta \; C\phi \end{bmatrix} $$

Similar relations may be developed for ${}_{LG}T_H$ and ${}_{RG}T_H$.

5.2.7 Gear Velocity to Gear

The transformation ${}_{jG}T_{jGV}$ is obtained directly from the relations developed in Sections 5.2.5 and 5.2.6. The transformation from the jth Gear velocity axis system to the jth gear axis system may be written

$$ {}_{jG}T_{jGV} = {}_{jG}T_H \cdot {}_H T_{jGV} \tag{5.2-46}$$

Where $_{H}T_{jGV}$ is used from expression (5.2-41) and $_{jG}T_{H}$ is used from relation (5.2-43) for the corresponding j^{th} gear.

5.2.8 Gear Velocity to Aircraft Body

The relations from Sections 5.2.4 are used with the relations from Section 5.2.7 to obtain the transform relation from the Gear Velocity axis system to the Aircraft's body axis system. Again, for the j^{th} gear the transform may be expressed:

$$_{B}T_{jGV} = {_{B}T_{jG}} \cdot {_{jG}T_{jGV}} \qquad (5.2\text{-}47)$$

where $_{jG}T_{jGV}$ is obtained from (5.2-46) and $_{B}T_{jG}$ is obtained from (5.2-33), (5.2-38) or (5.2-36) for the appropriate left, right or nose gear.

6.0 GEAR MODEL OUTPUT AND INPUT REQUIREMENTS

The output information from the gear model is the total forces and moments acting on the aircraft center of gravity as a result of the landing gear reactions.

The input information required to use the model to calculate this output takes two forms; continuously changing information which is the result of the aircraft's dynamic motion, and static data that describe the physical characteristics of the aircraft-gear-runway system.

6.1 GEAR MODEL OUTPUT

The results of the gear mathematical model are the forces and moments applied at the aircraft center of gravity by the combined landing gear system. Figure 3-5 shows the force system acting on the j^{th} tire. Obtaining the components of the force vector acting on the tire from equations (3.4.14), (3.3-1) and (3.2-4), the force vector $\overline{F}_{jGV}$ may be formulated as:

$$\overline{F}_{jGV} = \begin{Bmatrix} F_{jV1} \\ F_{jV2} \\ F_{jV3} \end{Bmatrix} \qquad (6.1\text{-}1)$$

This vector is expressed in the j^{th} gear velocity axis system. The transformation to the aircraft body axes is obtained from relation (4.2-46).

$$\overline{F}_{jA/C} = B^T{}_{jG \cdot V}\, \overline{F}_{jGV} \qquad (6.1\text{-}2)$$

This vector is now in the desired axis system. However, it is acting at the j^{th} wheel and not at the center of gravity of the aircraft. A force acting at the wheel is equivalent to a force acting at the center of gravity plus the moment about the center of gravity due to the force at the wheel. This moment may be calculated by taking the vector cross product of the radius vector from the center of gravity to the wheel into the force vector.

$$\overline{M}_{jA/C} = \overline{R}_j \cdot \overline{F}_{jA/C} \tag{6.1-3}$$

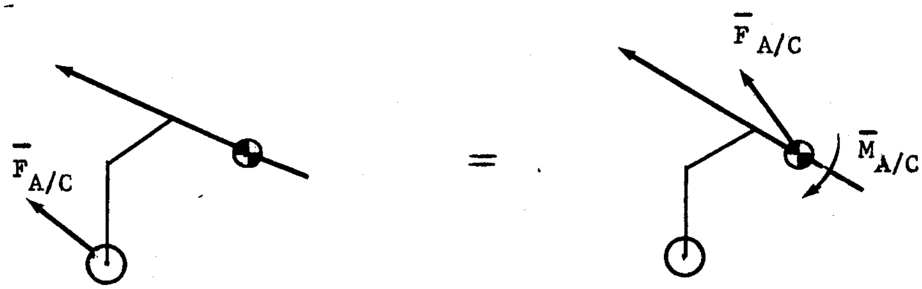

Force Equivalence Diagram

FIGURE 6-1

The vector $\overline{R}_j$ from the c.g. of the aircraft to the gear hub has components in the aircraft body axis system. This vector is determined at any instant of time by defining it as the sum of two vectors.

$$\overline{R}_j = \overline{R}_{jA} + \overline{R}_{jAW} \tag{6.1-4}$$

where $\overline{R}_{jA}$ is the radius vector to the gear attach point which is a fixed quantity, and $\overline{R}_{jAW}$ is the vector from the gear attach point to the wheel hub. $\overline{R}_{jAW}$ is determined at any instant of time by transforming a vector from the gear attach point to the wheel in the gear axis system, $\overline{\ell}_{jAW}$, into the aircraft body axis system.

$$\overline{R}_{jAW} = {}_B T_{jG} \cdot \overline{\ell}_{jAW} \tag{6.1-5}$$

where ${}_B T_{jG}$ is determined from the appropriate expression (5.2-33), (5.2-36) or (5.2-38), depending on the gear and simplifications involved.

In the gear axis system, the vector $\overline{\ell}_{jAW}$ is the instantaneous length of the strut along the gear Z axis from the attach point to the hub.

$$\overline{\ell}_{jAW} = \begin{Bmatrix} 0 \\ 0 \\ dj \end{Bmatrix} \qquad (6.1\text{-}6)$$

This length is determined by subtracting the strut deflection δ_{js} from the extended length d_{iE}

$$dj = d_{iE} - \delta_{js} \qquad (6.1\text{-}7)$$

The total force and moment acting at the aircraft's center of gravity as a result of gear action are obtained by vector summing the results of equations (6.1-2) and (6.1-3) over the three gears. Replacing the j with L for left gear, R for right gear and N for nose gear, these expressions are:

$$\overline{F}_G = \overline{F}_{LA/C} + \overline{F}_{RA/C} + \overline{F}_{NA/C} \qquad (6.1\text{-}8)$$

$$\overline{M}_G = \overline{M}_{LA/C} + \overline{M}_{RA/C} + \overline{M}_{NA/C} \qquad (6.1\text{-}9)$$

These are the forces and moments that must be summed with the aerodynamic and propulsion forces and moments acting on the vehicle to determine the dynamic behavior of the aircraft.

6.2 Dynamic Input Information

This information changes continuously as the aircraft performs its dynamic motion in response to the forces acting on the aircraft. Items that must be included are:

- o Aircraft translational velocities in local vertical (N.E.D.) coordinates ($\overline{V}_G$);
- o Aircraft pitch (θ), roll (ϕ) and yaw (ψ) attitude angles;
- o Aircraft position over the Earth, latitude and longitude;
- o Aircraft altitude; h_{cg}
- o Aircraft rotational velocities in body axes, (p,q,r).

The aircraft translational and rotational velocities are used to determine the velocities at the wheels as in equation (3.1-16). The aircraft attitudes are used with the altitude to determine the height of each wheel hub above the runway. In addition, the attitudes establish the transformations between the local vertical, the horizontal and the aircraft body axis systems. Finally, the aircraft position is used to determine the relative location along the runway and the lateral position on the runway as discussed in Section 4.1.

7.1 FIXED DATA

MATH NAME	FORTRAN SYMBOL	VALUE
A_{BRK}	ABRK	5.0 In^2
C_{TM}	ACMT	50.0 lb/In/Sec
C_{TN}	ACNT	50.0 lb/In/Sec
K_{TM}	AKMT	9030.0 lb/In
K_{TN}	AKNT	17300.0 lb/In
C_{DM}	CMD	200.0 lb/In/Sec
C_{DN}	CND	500.0 lb/In/Sec
d_{ME}	DME	7.125 ft
d_{NE}	DNE	6.975 ft
D_{XMALE}	DXMALE	5.778 ft
D_{XNALE}	DXNALE	37.189 ft
RMLA1	RMLA(1)	8.728 ft
RMLA2	RMLA(2)	-9.104 ft
RMLA3	RMLA(3)	1.60 ft
RMRA1	RMRA(1)	8.728 ft
RMRA2	RMRA(2)	9.104 ft
RMRA3	RMRA(3)	1.60 ft
RNA1	RNA(1)	40.139 ft
RNA2	RNA(2)	0.0 ft
RNA3	RNA(3)	1.59 ft
R_{TIM}	RTIM	20.10 In
R_{TIN}	RTIN	12.74 In
SFBUMP	SFBUMP	2.0 N/D
SFCROWN	SFCROWN	1.0 N/D
W_{TM}	WTM	900.0 lb
W_{TN}	WTN	276.0 lb

7.2 DYNAMIC DATA

The tables and figures in this section represent data that change with the dynamic condition of the aircraft. These data were included in the McAir computer program as table look up functions of the respective independent variables.

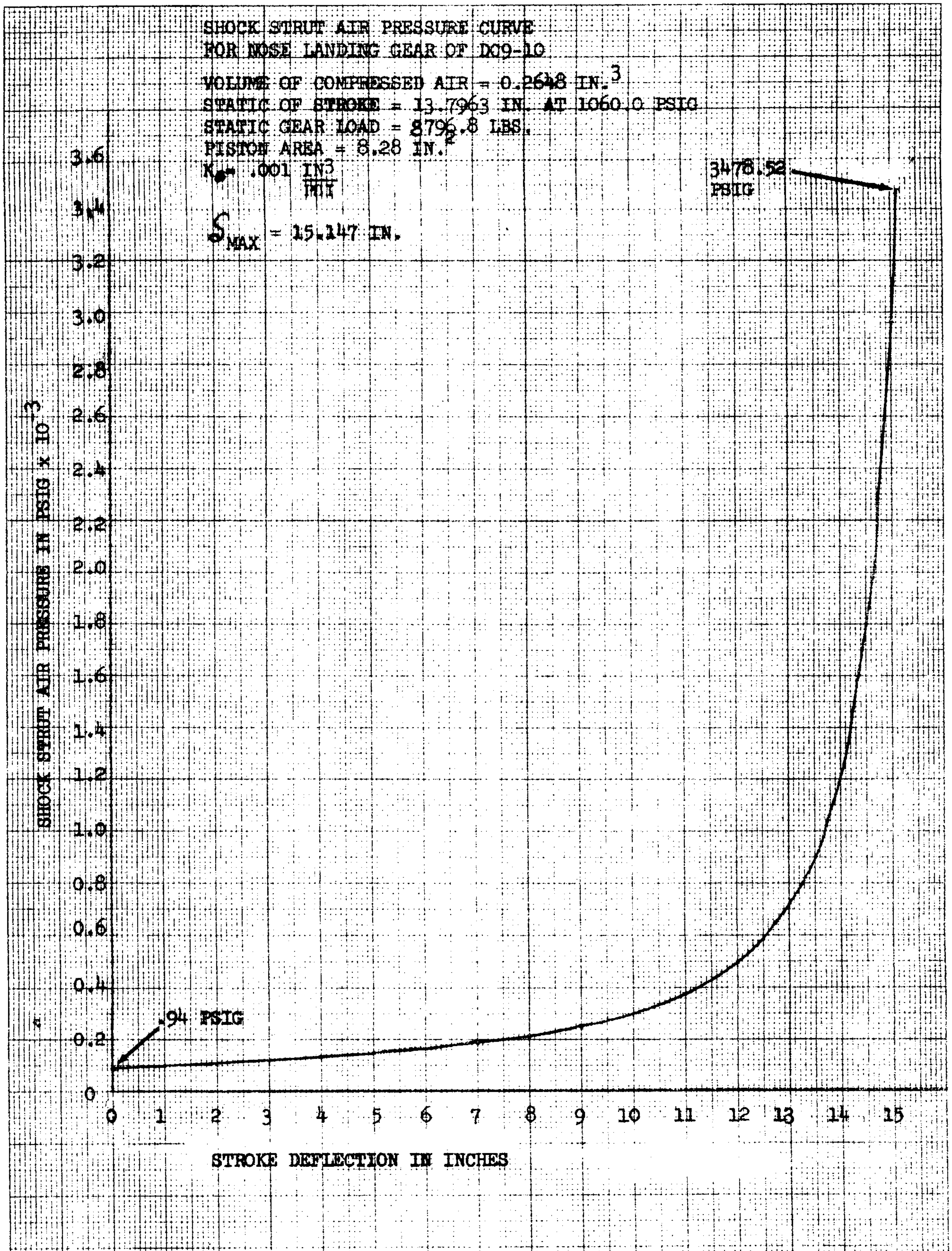
SHOCK STRUT AIR PRESSURE CURVE
FOR NOSE LANDING GEAR OF DC9-10
VOLUME OF COMPRESSED AIR = 0.2648 IN.3
STATIC OF STROKE = 13.7963 IN. AT 1060.0 PSIG
STATIC GEAR LOAD = 8796.8 LBS.
PISTON AREA = 8.28 IN.2
K = .001 IN3/PSI
δMAX = 15.147 IN.
3478.52 PSIG
.94 PSIG
SHOCK STRUT AIR PRESSURE IN PSIG x 10-3
STROKE DEFLECTION IN INCHES
0
0.2
0.4
0.6
0.8
1.0
1.2
1.4
1.6
1.8
2.0
2.2
2.4
2.6
2.8
3.0
3.2
3.4
3.6
0
1
2
3
4
5
6
7
8
9
10
11
12
13
14
15

FIGURE 7-1

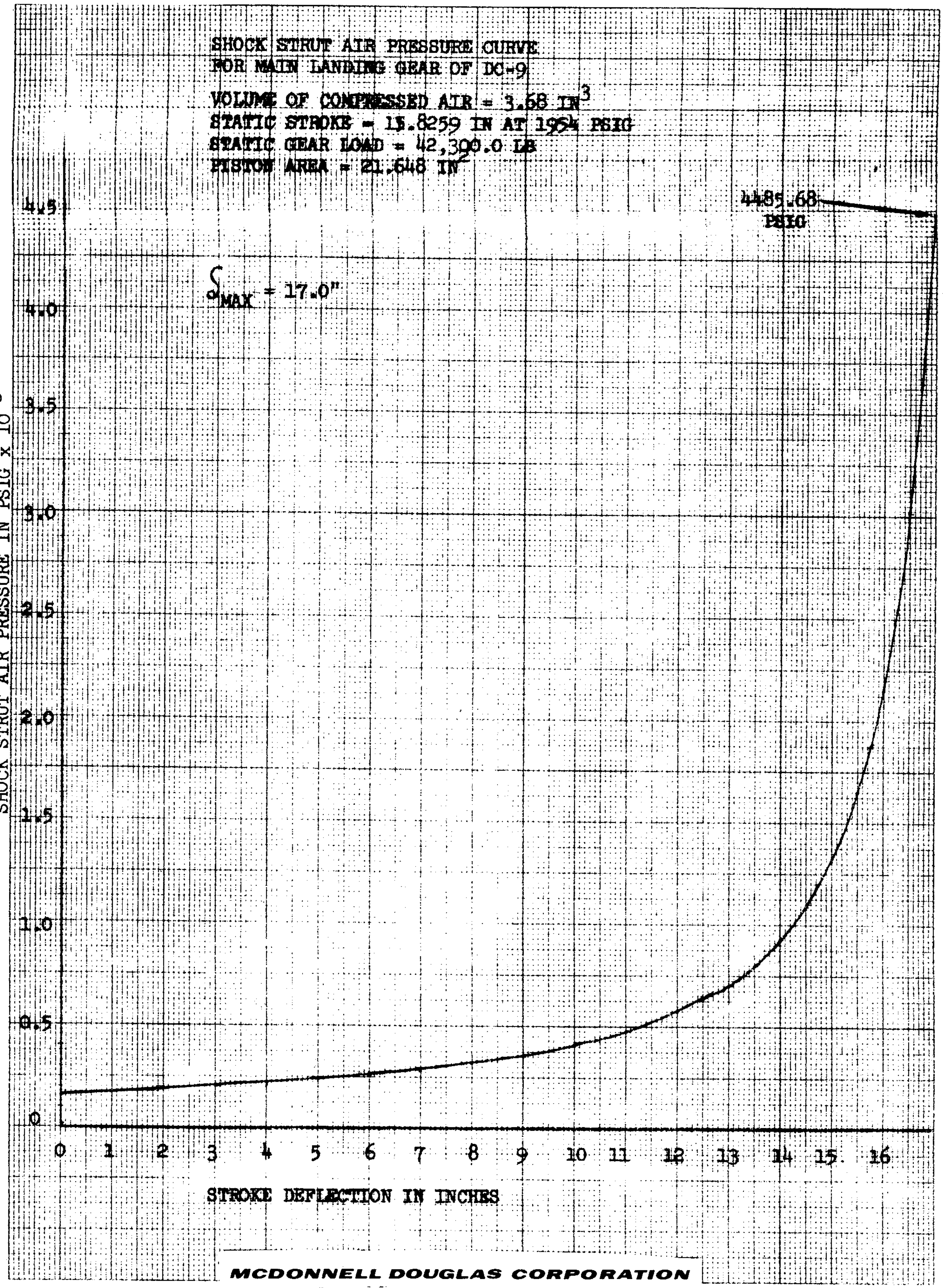
SHOCK STRUT AIR PRESSURE CURVE
FOR MAIN LANDING GEAR OF DC-9
VOLUME OF COMPRESSED AIR = 3.68 IN^3
STATIC STROKE = 15.8259 IN AT 1964 PSIG
STATIC GEAR LOAD = 42,300.0 LB
PISTON AREA = 21.648 IN^2
δMAX = 17.0"
4485.68 PSIG
SHOCK STRUT AIR PRESSURE IN PSIG x 10^-3
0
0.5
1.0
1.5
2.0
2.5
3.0
3.5
4.0
4.5
0 1 2 3 4 5 6 7 8 9 10 11 12 13 14 15 16
STROKE DEFLECTION IN INCHES

FIGURE 7-2

TABLE 7-1

RUNWAY PROFILE DATA

BUMP HEIGHT (in)	RUNWAY (feet)	BUMP HEIGHT (in)	RUNWAY (feet)	BUMP HEIGHT (in)	RUNWAY (feet)
		0.066	123.999	0.710	259.999
		0.009	125.999	0.733	261.999
		0.071	128.001	0.675	264.001
		-0.026	130.001	0.778	266.000
		0.017	132.001	0.642	268.000
		0.080	134.000	0.644	270.000
0.195	0.0	0.042	136.000	0.587	272.000
0.198	2.000	0.125	138.000	0.570	274.000
0.161	4.000	0.047	140.000	0.553	276.000
0.124	6.000	0.070	142.000	0.436	277.999
0.246	7.999	0.133	143.999	0.458	279.999
0.248	9.999	0.055	145.999	0.381	281.999
0.351	11.999	0.158	147.999	0.285	283.999
0.333	13.999	0.221	149.998	0.247	286.001
0.357	16.001	0.164	152.001	0.250	288.001
0.339	18.001	0.126	154.001	0.273	290.000
0.362	20.000	0.129	156.000	0.236	292.000
0.385	22.000	0.052	158.000	0.218	294.000
0.367	24.000	0.075	160.000	0.221	296.000
0.390	26.000	0.078	162.000	0.144	298.000
0.452	28.000	0.080	164.000	0.107	300.000
0.456	29.999	0.043	165.999	0.170	301.999
0.458	31.999	0.007	167.999	0.152	303.999
0.521	33.999	-0.051	169.999	0.175	305.999
0.563	35.999	0.031	171.999	0.098	307.998
0.626	38.001	-0.046	174.001	0.121	310.001
0.608	40.001	0.017	176.001	0.084	312.000
0.612	42.001	-0.020	178.000	0.106	314.000
0.614	44.000	0.063	180.000	0.089	316.000
0.617	46.000	0.065	182.000	0.052	318.000
0.460	48.000	0.028	184.000	0.055	320.000
0.543	50.000	0.010	186.000	0.017	322.000
0.605	52.000	-0.027	187.999	0.040	323.999
0.588	53.999	-0.023	189.999	0.102	325.999
0.591	55.999	-0.080	191.999	0.145	327.999
0.613	57.999	-0.118	193.999	0.148	329.999
0.616	59.998	-0.115	196.001	0.111	332.001
0.639	62.001	-0.072	198.001	0.173	334.000
0.582	64.001	-0.050	200.001	0.116	336.000
0.605	66.000	-0.107	202.000	0.139	338.000
0.547	68.000	-0.084	204.000	0.122	340.000
0.550	70.000	-0.141	206.000	0.144	342.000
0.493	72.000	-0.138	208.000	0.048	344.000
0.515	74.000	-0.156	210.000	0.110	345.999
0.498	75.999	-0.113	211.999	0.113	347.999
0.521	77.999	-0.150	213.999	0.115	349.999
0.584	79.999	-0.128	215.999	0.118	351.999
0.547	81.999	-0.045	218.001	0.021	354.001
0.529	84.001	-0.082	220.001	0.044	356.000
0.492	86.001	-0.020	222.001	-0.053	358.000
0.535	88.000	-0.077	224.000	-0.071	360.000
0.638	90.000	-0.014	226.000	-0.167	362.000
0.600	92.000	0.068	228.000	-0.124	364.000
0.603	94.000	0.091	230.000	-0.222	366.000
0.506	96.000	0.054	232.000	-0.218	368.000
0.389	97.999	0.136	233.999	-0.316	369.999
0.352	99.999	0.219	235.999	-0.333	371.999
0.334	101.999	0.142	237.999	-0.350	373.999
0.318	103.999	0.324	239.999	-0.367	376.001
0.380	106.001	0.367	242.001	-0.404	378.001
0.283	108.001	0.409	244.001	-0.461	380.000
0.226	110.001	0.372	246.000	-0.459	382.000
0.189	112.000	0.515	248.000	-0.496	384.000
0.132	114.000	0.497	250.000	-0.394	386.000
0.095	116.000	0.560	252.000	-0.390	388.000
0.038	118.000	0.622	254.000	-0.348	390.000
0.040	119.999	0.745	255.999	-0.366	391.999
0.083	121.999	0.787	257.999	-0.362	393.999

TABLE 7-1 (CONTINUED)

RUNWAY PROFILE DATA

BUMP HEIGHT (in)	RUNWAY (feet)	BUMP HEIGHT (in)	RUNWAY (feet)	BUMP HEIGHT (in)	RUNWAY (feet)
-0.360	395.999	0.624	531.999	-0.107	667.999
-0.277	397.999	0.587	534.001	-0.164	670.001
-0.234	400.001	0.629	536.001	-0.062	672.000
-0.291	402.000	0.632	538.000	-0.060	674.000
-0.329	404.000	0.655	540.000	0.003	676.000
-0.267	406.000	0.678	542.000	-0.014	678.000
-0.164	408.000	0.660	544.000	0.068	680.000
-0.201	410.000	0.663	546.000	-0.008	682.000
-0.139	412.000	0.686	548.000	-0.006	684.000
-0.196	413.999	0.688	549.999	-0.083	685.999
-0.153	415.999	0.671	551.999	-0.100	687.999
-0.190	417.999	0.634	553.999	-0.177	689.999
-0.188	419.999	0.537	555.999	-0.234	692.001
-0.185	422.001	0.579	558.001	-0.271	694.001
-0.242	424.000	0.563	560.000	-0.269	696.000
-0.259	426.000	0.485	562.000	-0.226	698.000
-0.296	428.000	0.508	564.000	-0.223	700.000
-0.254	430.000	0.471	566.000	-0.200	702.000
-0.271	432.000	0.454	568.000	-0.118	704.000
-0.228	434.000	0.397	570.000	-0.095	706.000
-0.226	435.999	0.379	571.999	-0.052	707.999
-0.163	437.999	0.322	573.999	-0.030	709.999
-0.160	439.999	0.285	575.999	0.033	711.999
-0.118	441.999	0.248	577.999	-0.005	713.998
-0.115	444.001	0.251	580.001	0.078	716.001
-0.072	446.001	0.293	582.000	-0.019	718.000
-0.029	448.000	0.216	584.000	0.023	720.000
0.013	450.000	0.219	586.000	0.086	722.000
0.056	452.000	0.162	588.000	0.189	724.000
0.119	454.000	0.144	590.000	0.232	726.000
0.141	456.000	0.148	592.000	0.214	728.000
0.223	458.000	0.150	593.999	0.217	729.999
0.226	459.999	0.153	595.999	0.179	731.999
0.328	461.999	0.116	597.999	0.262	733.999
0.312	463.999	0.058	599.999	0.245	735.999
0.414	465.998	0.042	602.001	0.288	738.001
0.357	468.001	0.005	604.000	0.290	740.000
0.399	470.000	-0.052	606.000	0.373	742.000
0.402	472.000	-0.070	608.000	0.435	744.000
0.425	474.000	-0.047	610.000	0.378	746.000
0.488	476.000	-0.064	612.000	0.461	748.000
0.470	478.000	-0.061	614.000	0.444	750.000
0.492	480.000	-0.159	616.000	0.466	751.999
0.496	481.999	-0.116	617.999	0.409	753.999
0.538	483.999	-0.213	619.999	0.391	755.999
0.481	485.999	-0.230	621.999	0.334	757.999
0.563	487.999	-0.228	623.998	0.297	760.001
0.587	490.001	-0.165	626.001	0.220	762.000
0.589	492.000	-0.261	628.000	0.203	764.000
0.652	494.000	-0.200	630.000	0.146	766.000
0.674	496.000	-0.237	632.000	0.049	768.000
0.757	498.000	-0.214	634.000	0.052	770.000
0.680	500.000	-0.171	636.000	-0.125	772.000
0.643	502.000	-0.188	638.000	-0.122	774.000
0.586	503.999	-0.105	639.999	-0.239	775.999
0.568	505.999	-0.162	641.999	-0.355	777.999
0.511	507.999	-0.180	643.999	-0.453	779.999
0.494	509.999	-0.237	645.999	-0.510	781.998
0.497	512.001	-0.234	648.001	-0.607	784.001
0.539	514.000	-0.212	650.000	-0.744	786.000
0.562	516.000	-0.269	652.000	-0.821	788.000
0.505	518.000	-0.306	654.000	-0.897	790.000
0.587	520.000	-0.323	656.000	-0.915	792.000
0.490	522.000	-0.281	658.000	-0.972	794.000
0.553	524.000	-0.298	660.000	-1.009	796.000
0.536	526.000	-0.175	661.999	-1.046	797.999
0.638	527.999	-0.212	663.999	-1.064	799.999
0.561	529.999	-0.130	665.999	-1.040	801.999

TABLE 7-1 (CONTINUED)

RUNWAY PROFILE DATA

BUMP HEIGHT (in)	RUNWAY (feet)	BUMP HEIGHT (in)	RUNWAY (feet)	BUMP HEIGHT (in)	RUNWAY (feet)
-1.097	803.999	-0.592	940.001	-0.207	1076.001
-1.135	806.001	-0.590	942.001	-0.164	1078.000
-1.172	808.000	-0.627	944.000	-0.182	1080.000
-1.109	810.000	-0.604	946.000	-0.099	1082.000
-1.207	812.000	-0.602	948.000	-0.156	1084.000
-1.104	814.000	-0.619	950.000	-0.094	1086.000
-1.122	816.000	-0.596	952.000	-0.091	1088.000
-1.059	818.000	-0.534	954.000	0.012	1090.000
-1.036	819.999	-0.511	955.999	-0.026	1091.999
-1.093	821.999	-0.489	957.999	0.017	1093.999
-1.090	823.999	-0.546	959.999	0.020	1095.999
-1.108	825.999	-0.443	961.999	0.062	1098.001
-1.145	828.001	-0.500	964.001	0.065	1100.001
-1.202	830.000	-0.437	966.000	0.107	1102.000
-1.279	832.000	-0.394	968.000	0.210	1104.000
-1.276	834.000	-0.372	970.000	0.233	1106.000
-1.253	836.000	-0.409	972.000	0.255	1108.000
-1.211	838.000	-0.466	974.000	0.278	1110.000
-1.168	840.000	-0.404	976.000	0.361	1112.000
-1.185	841.999	-0.381	977.999	0.383	1113.999
-1.183	843.999	-0.378	979.999	0.366	1115.999
-1.160	845.999	-0.476	981.999	0.468	1117.999
-1.197	847.999	-0.373	983.999	0.531	1119.999
-1.134	850.001	-0.430	986.001	0.474	1122.001
-1.112	852.001	-0.348	988.000	0.497	1124.000
-1.109	854.000	-0.385	990.000	0.838	1126.000
-1.126	856.000	-0.382	992.000	0.961	1128.000
-1.084	858.000	-0.419	994.000	0.964	1130.000
-1.021	860.000	-0.357	996.000	1.026	1132.000
-1.078	862.000	-0.314	998.000	1.068	1134.000
-1.056	864.000	-0.351	999.999	1.051	1135.999
-1.153	865.999	-0.349	1001.999	0.994	1137.999
-1.050	867.999	-0.406	1003.999	0.957	1139.999
-1.068	869.999	-0.343	1005.999	0.920	1141.999
-0.985	871.998	-0.400	1008.001	0.923	1144.001
-0.962	874.001	-0.417	1010.001	0.846	1146.000
-0.959	876.000	-0.454	1012.000	0.809	1148.000
-0.877	878.000	-0.492	1014.000	0.711	1150.000
-0.855	880.000	-0.488	1016.000	0.694	1152.000
-0.831	882.000	-0.506	1018.000	0.597	1154.000
-0.809	884.000	-0.543	1020.000	0.560	1156.000
-0.806	886.000	-0.580	1022.000	0.464	1157.999
-0.823	887.999	-0.617	1023.999	0.446	1159.999
-0.760	889.999	-0.674	1025.999	0.369	1161.999
-0.778	891.999	-0.652	1027.999	0.352	1163.999
-0.815	893.999	-0.689	1029.998	0.275	1166.001
-0.713	896.001	-0.646	1032.001	0.278	1168.001
-0.730	898.000	-0.664	1034.000	0.201	1170.000
-0.687	900.000	-0.621	1036.000	0.203	1172.000
-0.685	902.000	-0.618	1038.000	0.146	1174.000
-0.761	904.000	-0.616	1040.000	0.109	1176.000
-0.779	906.000	-0.652	1042.000	0.152	1178.000
-0.736	908.000	-0.630	1044.000	0.095	1180.000
-0.714	909.999	-0.647	1045.999	0.058	1181.999
-0.690	911.999	-0.604	1047.999	0.021	1183.999
-0.688	913.999	-0.602	1049.999	-0.056	1185.999
-0.645	915.999	-0.619	1051.999	-0.054	1187.998
-0.603	918.001	-0.616	1054.001	0.009	1190.001
-0.580	920.000	-0.613	1056.000	-0.008	1192.000
-0.597	922.000	-0.611	1058.000	-0.026	1194.000
-0.694	924.000	-0.509	1060.000	-0.043	1196.000
-0.711	926.000	-0.466	1062.000	-0.061	1198.000
-0.709	928.000	-0.383	1064.000	-0.137	1200.000
-0.606	930.000	-0.361	1066.000	-0.075	1202.000
-0.604	932.000	-0.298	1067.999	-0.092	1203.999
-0.601	933.999	-0.295	1069.999	-0.049	1205.999
-0.658	935.999	-0.253	1071.999	-0.166	1207.999
-0.596	937.999	-0.250	1073.999	-0.104	1209.999

TABLE 7-1 (CONTINUED)

RUNWAY PROFILE DATA

BUMP HEIGHT (in)	RUNWAY (feet)	BUMP HEIGHT (in)	RUNWAY (feet)	BUMP HEIGHT (in)	RUNWAY (feet)
-0.161	1212.001	0.344	1348.001	-0.626	1484.000
-0.138	1214.000	0.287	1350.000	-0.623	1486.000
-0.175	1216.000	0.390	1352.000	-0.580	1488.000
-0.152	1218.000	0.453	1354.000	-0.598	1490.000
-0.190	1220.000	0.455	1356.000	-0.535	1492.000
-0.207	1222.000	0.478	1358.000	-0.633	1494.000
-0.144	1224.000	0.540	1360.000	-0.570	1496.000
-0.062	1225.999	0.623	1361.999	-0.587	1497.999
-0.099	1227.999	0.566	1363.999	-0.564	1499.999
-0.116	1229.999	0.668	1365.999	-0.641	1501.999
-0.114	1231.999	0.691	1367.999	-0.579	1503.998
-0.110	1234.001	0.713	1370.001	-0.616	1506.001
-0.128	1236.000	0.696	1372.000	-0.633	1508.000
-0.145	1238.000	0.699	1374.000	-0.670	1510.000
-0.163	1240.000	0.722	1376.000	-0.687	1512.000
-0.120	1242.000	0.684	1378.000	-0.645	1514.000
-0.157	1244.000	0.727	1380.000	-0.702	1516.000
-0.194	1246.000	0.670	1382.000	-0.699	1518.000
-0.251	1248.000	0.673	1383.999	-0.696	1519.999
-0.249	1249.999	0.636	1385.999	-0.634	1521.999
-0.325	1251.999	0.659	1387.999	-0.651	1523.999
-0.363	1253.999	0.641	1389.999	-0.629	1525.999
-0.339	1256.001	0.604	1392.001	-0.625	1528.001
-0.337	1258.001	0.587	1394.000	-0.682	1530.000
-0.354	1260.000	0.550	1396.000	-0.620	1532.000
-0.392	1262.000	0.532	1398.000	-0.657	1534.000
-0.368	1264.000	0.455	1400.000	-0.615	1536.000
-0.425	1266.000	0.498	1402.000	-0.612	1538.000
-0.463	1268.000	0.421	1404.000	-0.649	1540.000
-0.520	1270.000	0.483	1406.000	-0.686	1541.999
-0.577	1271.999	0.426	1407.999	-0.723	1543.999
-0.614	1273.999	0.429	1409.999	-0.801	1545.999
-0.671	1275.999	0.412	1411.999	-1.436	1547.999
-0.708	1277.999	0.395	1414.001	-0.795	1550.001
-0.745	1280.001	0.378	1416.001	-0.732	1552.000
-0.782	1282.000	0.340	1418.000	-0.690	1554.000
-0.860	1284.000	0.323	1420.000	-0.627	1556.000
-0.857	1286.000	0.266	1422.000	-0.505	1558.000
-0.894	1288.000	0.229	1424.000	-0.502	1560.000
-0.852	1290.000	0.192	1426.000	-0.419	1562.000
-0.888	1292.000	0.135	1428.000	-0.357	1563.999
-0.886	1293.999	0.118	1429.999	-0.354	1565.999
-0.864	1295.999	0.121	1431.999	-0.391	1567.999
-0.880	1297.999	0.083	1433.999	-0.369	1569.999
-0.858	1299.999	0.046	1435.998	-0.366	1572.001
-0.855	1302.001	-0.031	1438.001	-0.363	1574.001
-0.832	1304.000	-0.028	1440.000	-0.381	1576.000
-0.830	1306.000	-0.065	1442.000	-0.398	1578.000
-0.747	1308.000	-0.122	1444.000	-0.375	1580.000
-0.645	1310.000	-0.160	1446.000	-0.412	1582.000
-0.542	1312.000	-0.256	1448.000	-0.429	1584.000
-0.480	1314.000	-0.274	1450.000	-0.427	1586.000
-0.437	1315.999	-0.331	1451.999	-0.443	1587.999
-0.355	1317.999	-0.308	1453.999	-0.401	1589.999
-0.312	1319.999	-0.346	1455.999	-0.419	1591.999
-0.210	1321.999	-0.403	1457.999	-0.415	1593.998
-0.186	1324.001	-0.379	1460.001	-0.413	1596.001
-0.105	1326.001	-0.436	1462.000	-0.390	1598.000
-0.121	1328.000	-0.434	1464.000	-0.427	1600.000
0.021	1330.000	-0.471	1466.000	-0.405	1602.000
0.023	1332.000	-0.469	1468.000	-0.422	1604.000
0.027	1334.000	-0.506	1470.000	-0.439	1606.000
0.088	1336.000	-0.503	1472.000	-0.436	1608.000
0.092	1338.000	-0.540	1473.999	-0.434	1609.999
0.174	1339.999	-0.537	1475.999	-0.371	1611.999
0.157	1341.999	-0.555	1477.999	-0.349	1613.999
0.279	1343.999	-0.571	1479.999	-0.326	1615.999
0.282	1345.998	-0.589	1482.001	-0.323	1618.001

TABLE 7-1 (CONTINUED)

RUNWAY PROFILE DATA

BUMP HEIGHT (in)	RUNWAY (feet)	BUMP HEIGHT (in)	RUNWAY (feet)	BUMP HEIGHT (in)	RUNWAY (feet)
-0.260	1620.000	0.245	1755.991	-0.267	1891.991
-0.238	1622.000	0.247	1757.991	-0.244	1893.991
-0.156	1624.000	0.210	1759.991	-0.281	1895.991
-0.093	1626.000	0.193	1761.991	-0.239	1897.991
-0.090	1628.000	0.235	1763.991	-0.196	1899.991
0.012	1630.000	0.178	1765.991	-0.133	1901.991
0.015	1631.999	0.161	1767.991	-0.131	1903.991
0.118	1633.999	0.104	1769.991	0.071	1905.991
0.160	1635.991	0.087	1771.991	0.094	1907.991
0.223	1637.991	0.070	1773.991	0.176	1909.991
0.345	1639.991	0.053	1775.991	0.279	1911.991
0.388	1641.991	0.075	1777.991	0.361	1913.991
0.431	1643.991	0.038	1779.991	0.464	1915.991
0.453	1645.991	0.041	1781.991	0.446	1917.991
0.555	1647.991	-0.036	1783.991	0.609	1919.991
0.579	1649.991	0.026	1785.991	0.692	1921.991
0.681	1651.991	-0.011	1787.991	0.753	1923.991
0.624	1653.991	-0.028	1789.991	0.757	1925.991
0.726	1655.991	-0.045	1791.991	0.819	1927.991
0.689	1657.991	-0.062	1793.991	0.901	1929.991
0.731	1659.991	-0.040	1795.991	0.924	1931.991
0.735	1661.991	-0.077	1797.991	0.986	1933.991
0.757	1663.991	-0.054	1799.991	1.009	1935.991
0.800	1665.991	-0.052	1801.991	1.132	1937.991
0.802	1667.991	0.011	1803.991	1.055	1939.991
0.805	1669.991	-0.026	1805.991	1.137	1941.991
0.828	1671.991	0.037	1807.991	1.120	1943.991
0.810	1673.991	0.019	1809.991	1.143	1945.991
0.793	1675.991	0.042	1811.991	1.165	1947.991
0.856	1677.991	0.085	1813.991	1.268	1949.991
0.878	1679.991	0.128	1815.991	1.151	1951.991
0.901	1681.991	0.170	1817.991	1.274	1953.991
0.923	1683.991	0.193	1819.991	1.356	1955.991
0.886	1685.991	0.215	1821.991	1.278	1957.991
1.009	1687.991	0.199	1823.991	1.221	1959.991
0.912	1689.991	0.221	1825.991	1.264	1961.991
0.915	1691.991	0.203	1827.991	1.347	1963.991
0.918	1693.991	0.186	1829.991	1.369	1965.991
0.900	1695.991	0.189	1831.991	1.871	1967.991
0.804	1697.991	0.152	1833.991	2.093	1969.991
0.806	1699.991	0.174	1835.991	2.056	1971.991
0.829	1701.991	0.157	1837.991	1.959	1973.991
0.792	1703.991	0.180	1839.991	1.981	1975.991
0.775	1705.991	0.143	1841.991	1.944	1977.991
0.698	1707.991	0.145	1843.991	2.107	1979.991
0.720	1709.991	0.129	1845.991	2.149	1981.991
0.663	1711.991	0.131	1847.991	2.152	1983.991
0.686	1713.991	0.114	1849.991	2.035	1985.991
0.649	1715.991	0.177	1851.991	1.978	1987.991
0.651	1717.991	0.159	1853.991	1.921	1989.991
0.694	1719.991	0.122	1855.991	1.884	1991.991
0.636	1721.991	0.145	1857.991	1.746	1993.991
0.640	1723.991	0.088	1859.991	1.709	1995.991
0.603	1725.991	0.130	1861.991	1.593	1997.991
0.585	1727.991	0.054	1863.991	1.436	1999.991
0.528	1729.991	0.016	1865.991	1.359	2001.991
0.531	1731.991	-0.001	1867.991	1.242	2003.991
0.534	1733.991	-0.018	1869.991	1.185	2005.991
0.477	1735.991	-0.056	1871.991	1.108	2007.991
0.499	1737.991	-0.093	1873.991	1.051	2009.991
0.422	1739.991	-0.070	1875.991	0.994	2011.991
0.505	1741.991	-0.127	1877.991	0.937	2013.991
0.388	1743.991	-0.144	1879.991	0.880	2015.991
0.411	1745.991	-0.201	1881.991	0.823	2017.991
0.333	1747.991	-0.118	1883.991	0.766	2019.991
0.336	1749.991	-0.175	1885.991	0.768	2021.991
0.260	1751.991	-0.232	1887.991	0.811	2023.991
0.282	1753.991	-0.210	1889.991	0.753	2025.991

TABLE 7-1 (CONTINUED)

RUNWAY PROFILE DATA

BUMP HEIGHT (in)	RUNWAY (feet)	BUMP HEIGHT (in)	RUNWAY (feet)	BUMP HEIGHT (in)	RUNWAY (feet)
0.776	2027.991	-0.433	2163.991	-0.786	2299.991
0.719	2029.991	-0.471	2165.991	-0.803	2301.991
0.802	2031.991	-0.468	2167.991	-0.800	2303.991
0.804	2033.991	-0.485	2169.991	-0.778	2305.991
0.828	2035.991	-0.542	2171.991	-0.815	2307.991
0.770	2037.991	-0.539	2173.991	-0.832	2309.991
0.753	2039.991	-0.576	2175.991	-0.789	2311.991
0.775	2041.991	-0.594	2177.991	-0.766	2313.991
0.818	2043.991	-0.631	2179.991	-0.783	2315.991
0.841	2045.991	-0.588	2181.991	-0.801	2317.991
0.803	2047.991	-0.605	2183.991	-0.738	2319.991
0.807	2049.991	-0.623	2185.991	-0.716	2321.991
0.829	2051.991	-0.640	2187.991	-0.693	2323.991
0.872	2053.991	-0.617	2189.991	-0.670	2325.991
0.874	2055.991	-0.615	2191.991	-0.627	2327.991
0.837	2057.991	-0.611	2193.991	-0.585	2329.991
0.780	2059.991	-0.669	2195.991	-0.562	2331.991
0.743	2061.991	-0.666	2197.991	-0.460	2333.991
0.686	2063.991	-0.644	2199.991	-0.477	2335.991
0.688	2065.991	-0.661	2201.991	-0.414	2337.991
0.672	2067.991	-0.618	2203.991	-0.332	2339.991
0.655	2069.991	-0.635	2205.991	-0.329	2341.991
0.677	2071.991	-0.612	2207.991	-0.327	2343.991
0.600	2073.991	-0.630	2209.991	-0.284	2345.991
0.563	2075.991	-0.647	2211.991	-0.262	2347.991
0.545	2077.991	-0.624	2213.991	-0.239	2349.991
0.469	2079.991	-0.681	2215.991	-0.156	2351.991
0.431	2081.991	-0.718	2217.991	-0.154	2353.991
0.374	2083.991	-0.676	2219.991	-0.051	2355.991
0.357	2085.991	-0.673	2221.991	-0.108	2357.991
0.280	2087.991	-0.731	2223.991	-0.045	2359.991
0.283	2089.991	-0.688	2225.991	-0.043	2361.991
0.186	2091.991	-0.705	2227.991	0.020	2363.991
0.229	2093.991	-0.702	2229.991	0.002	2365.991
0.151	2095.991	-0.679	2231.991	0.005	2367.991
0.135	2097.991	-0.697	2233.991	0.048	2369.991
0.077	2099.991	-0.634	2235.991	0.030	2371.991
0.060	2101.991	-0.651	2237.991	0.073	2373.991
0.043	2103.991	-0.608	2239.991	0.016	2375.991
-0.054	2105.991	-0.586	2241.991	0.158	2377.991
-0.051	2107.991	-0.583	2243.991	0.101	2379.991
-0.088	2109.991	-0.580	2245.991	0.164	2381.991
0.093	2111.991	-0.578	2247.991	0.186	2383.991
0.077	2113.991	-0.495	2249.991	0.169	2385.991
0.119	2115.991	-0.513	2251.991	0.212	2387.991
0.142	2117.991	-0.470	2253.991	0.195	2389.991
0.125	2119.991	-0.527	2255.991	0.257	2391.991
0.168	2121.991	-0.444	2257.991	0.181	2393.991
0.130	2123.991	-0.462	2259.991	0.263	2395.991
0.113	2125.991	-0.359	2261.991	0.186	2397.991
0.036	2127.991	-0.377	2263.991		
0.019	2129.991	-0.334	2265.991		
0.001	2131.991	-0.371	2267.991		
-0.016	2133.991	-0.388	2269.991		
-0.113	2135.991	-0.365	2271.991		
-0.090	2137.991	-0.402	2273.991		
-0.128	2139.991	-0.400	2275.991		
-0.144	2141.991	-0.437	2277.991		
-0.161	2143.991	-0.435	2279.991		
-0.218	2145.991	-0.511	2281.991		
-0.196	2147.991	-0.488	2283.991		
-0.253	2149.991	-0.525	2285.991		
-0.251	2151.991	-0.582	2287.991		
-0.308	2153.991	-0.600	2289.991		
-0.325	2155.991	-0.697	2291.991		
-0.382	2157.991	-0.654	2293.991		
-0.359	2159.991	-0.692	2295.991		
-0.416	2161.991	-0.689	2297.991		

TABLE 7-2

NOSE STRUT VELOCITY SQUARED DAMPING COEFFICIENTS

Strut Compression (IN)	Coefficient	
0.0	0.109	
0.49	0.668	
8.37	1.742	+ 10.6 (strut extending)
12.75	5.671	
15.15	8.310	

TABLE 7-3

MAIN STRUT VELOCITY SQUARED DAMPING COEFFICIENTS

Strut Compression (IN)	Coefficient	
0.0	2.50	
6.0	3.21	+ 93.7 (strut extending)
12.0	14.98	
17.0	42.73	

DISTANCE FROM RUNWAY THRESHOLD, FT	CASE 1			CASE #2			CASE #3			CASE #4		
	LMG	NG	RMG	LMG	NG	RMG	LMG	NG	RMG	LMG	NG	RMG
0 - 500	DRY	DRY	DRY	DRY	DRY	DRY	WET	WET	WET	WET	WET	WET
501 - 1000	DRY	DRY	DRY	DRY	DRY	DRY	WET	WET	WET	WET	WET	WET
1001 - 1500	DRY	DRY	DRY	DRY	DRY	DRY	WET	WET	WET	WET	WET	WET
1501 - 2000	DRY	DRY	DRY	DRY	DRY	DRY	WET	WET	WET	WET	WET	WET
2001 - 2500	DRY	DRY	DRY	DRY	DRY	DRY	WET	WET	WET	WET	WET	WET
2501 - 3000	DRY	DRY	DRY	DRY	DRY	DRY	WET	WET	WET	WET	WET	WET
3001 - 3500	DRY	DRY	DRY	DRY	DRY	DRY	WET	WET	WET	WET	WET	WET
3501 - 4000	DRY	DRY	DRY	DRY	DRY	DRY	WET	WET	WET	WET	WET	WET
4001 - 4500	WET	WET	WET	WET	WET	DRY	FLOODED	FLOODED	FLOODED	FLOODED	WET	WET
4501 - 5000	DRY	DRY	DRY	DRY	DRY	DRY	WET	WET	WET	WET	WET	ICE
5001 - 5050	WET	WET	WET	WET	DRY	DRY	FLOODED	FLOODED	FLOODED	ICE	ICE	WET
5051 - 5100	DRY	DRY	DRY	WET	DRY	WET	WET	WET	WET	WET	WET	FLOODED
5101 - 5150	WET	WET	WET	FLOODED	WET	WET	FLOODED	FLOODED	FLOODED	ICE	ICE	WET
5151 - 5200	DRY	DRY	DRY	FLOODED	WET	WET	WET	WET	WET	WET	WET	FLOODED
5201 - 5250	WET	WET	WET	WET	WET	WET	DRY	DRY	DRY	FLOODED	WET	WET
5251 - 5300	FLOODED	FLOODED	FLOODED	DRY	DRY	DRY	FLOODED	FLOODED	FLOODED	WET	WET	ICE
5301 - 5350	WET	WET	WET	DRY	DRY	DRY	WET	WET	WET	ICE	ICE	WET
5351 - 5400	DRY	DRY	DRY	WET	DRY	DRY	FLOODED	FLOODED	FLOODED	WET	WET	FLOODED
5401 - 5450	DRY	DRY	DRY	WET	WET	WET	WET	WET	WET	ICE	ICE	WET
5451 - 5500	DRY	DRY	DRY	FLOODED	WET	WET	DRY	DRY	DRY	WET	WET	FLOODED
5501 - 5600	WET	WET	WET	WET	DRY	WET	WET	WET	WET	FLOODED	WET	WET
5601 - 5700	DRY	DRY	DRY	WET	DRY	WET	FLOODED	FLOODED	FLOODED	WET	WET	FLOODED
5701 - 5800	WET	WET	WET	FLOODED	WET	WET	WET	WET	WET	FLOODED	WET	WET
5801 - 5900	DRY	DRY	DRY	FLOODED	WET	WET	DRY	DRY	DRY	WET	WET	FLOODED
5901 - 6000	WET	WET	WET	FLOODED	FLOODED	FLOODED	WET	WET	WET	FLOODED	WET	WET
6001 - 6500	DRY	DRY	DRY	WET	WET	WET	FLOODED	FLOODED	FLOODED	WET	WET	FLOODED
6501 - 7000	WET	WET	WET	WET	WET	WET	WET	WET	WET	FLOODED	WET	WET
7001 - 7500	FLOODED	FLOODED	FLOODED	DRY	DRY	DRY	DRY	DRY	DRY	WET	WET	FLOODED
7501 - 8000	WET	WET	WET	WET	DRY	DRY	WET	WET	WET	FLOODED	WET	WET
8001 - 8500	DRY	DRY	DRY	DRY	DRY	DRY	FLOODED	FLOODED	FLOODED	WET	WET	FLOODED
8501 - 9000	WET	WET	WET	WET	WET	WET	WET	WET	WET	FLOODED	WET	WET
9001 - 9500	DRY	DRY	DRY	DRY	DRY	DRY	WET	WET	WET	WET	WET	FLOODED
9501 - 10000	WET	WET	WET	WET	DRY	DRY	WET	WET	WET	FLOODED	WET	WET
	TOUCHDOWN-DRY SYMMETRIC			TOUCHDOWN-DRY UNSYMMETRIC			TOUCHDOWN-WET SYMMETRIC			TOUCHDOWN-WET UNSYMMETRIC		
LMG - LEFT MAIN GEAR NG - NOSE GEAR RMG - RIGHT MAIN GEAR												

FIGURE 7-3
PATCHY RUNWAY CONDITION PROFILES

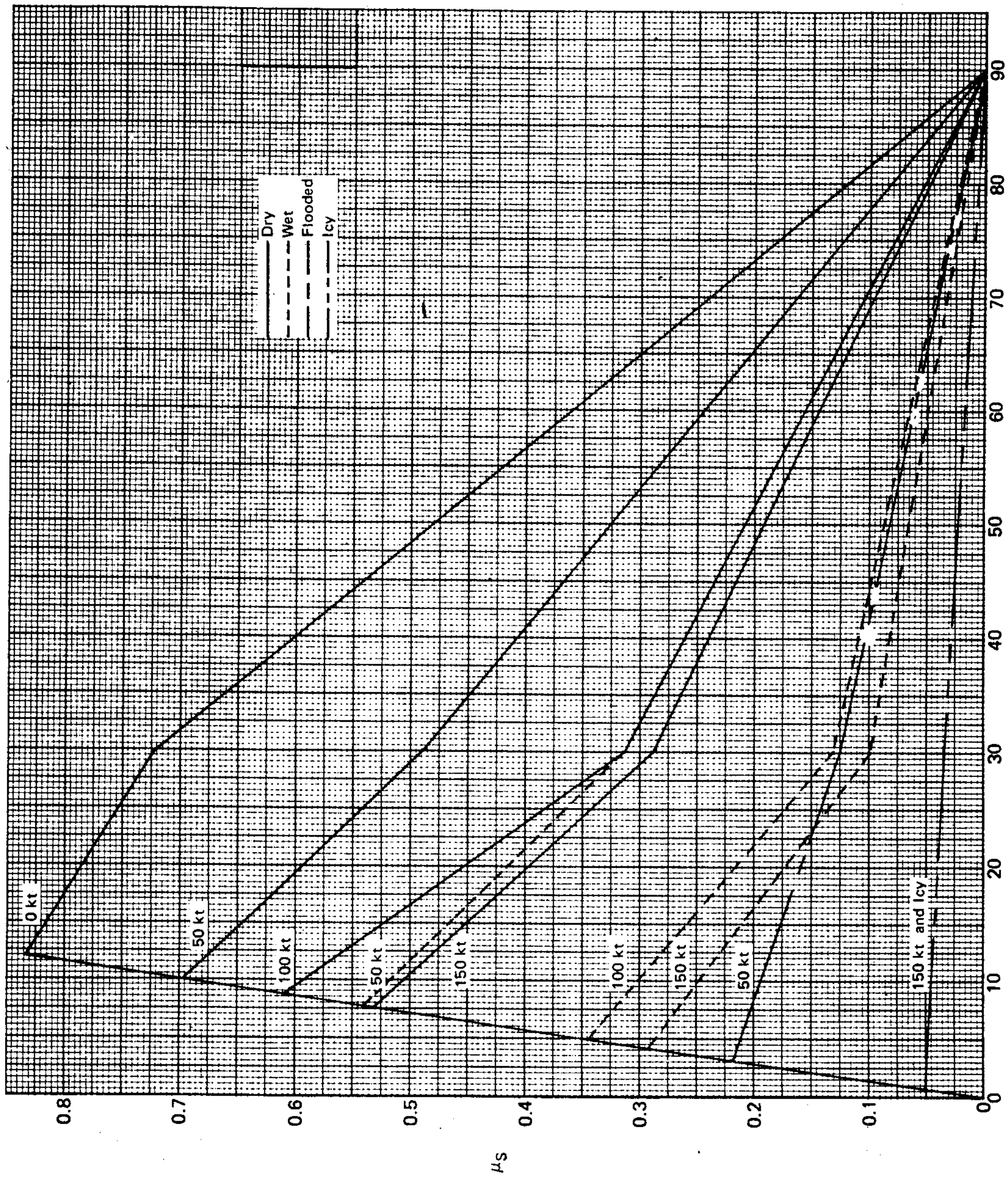

FIGURE 7-4
DC-9 NOSE TIRE CORNERING COEFFICIENT

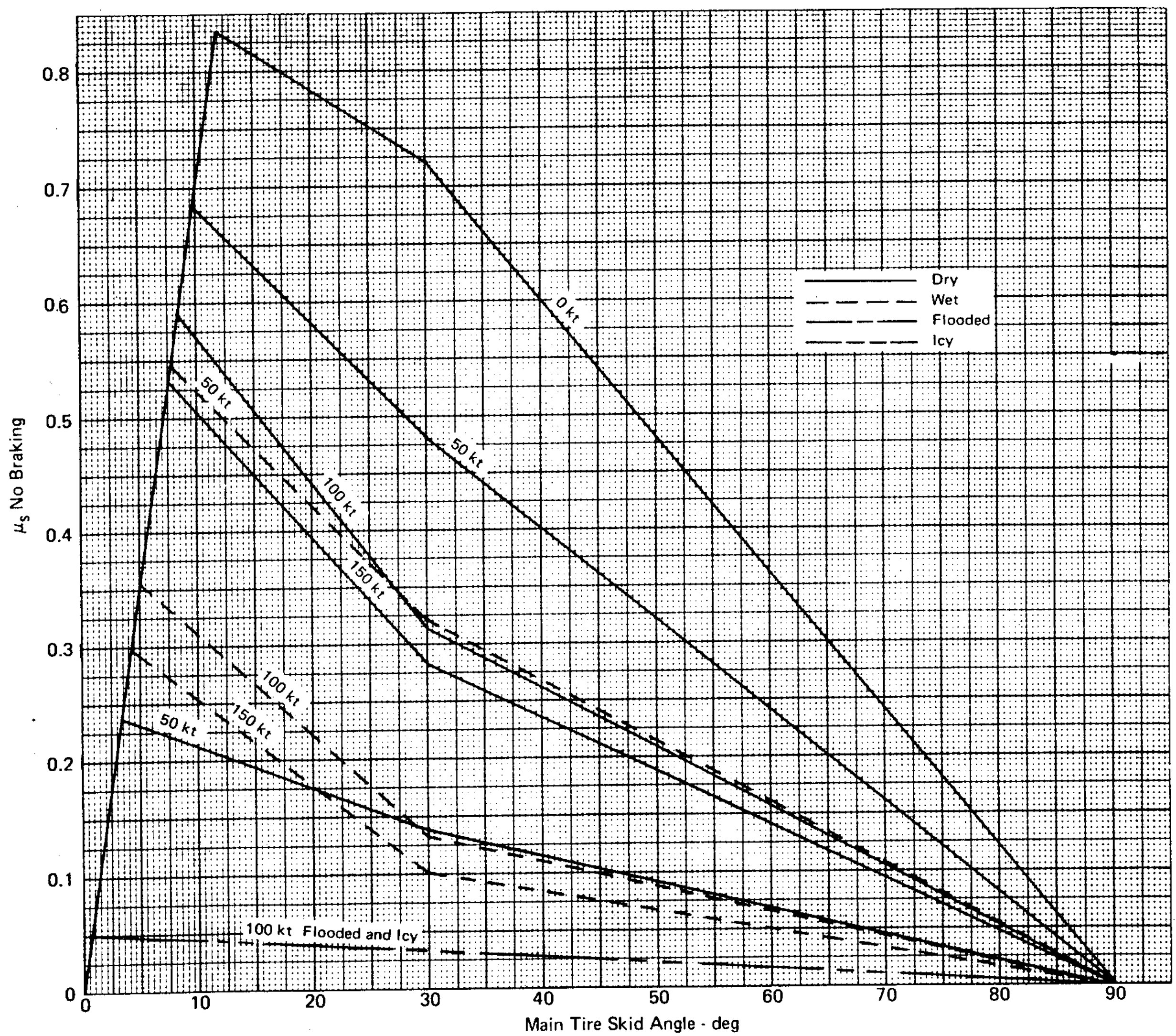

FIGURE 7-5
DC-9 MAIN TIRE CORNERING COEFFICIENT

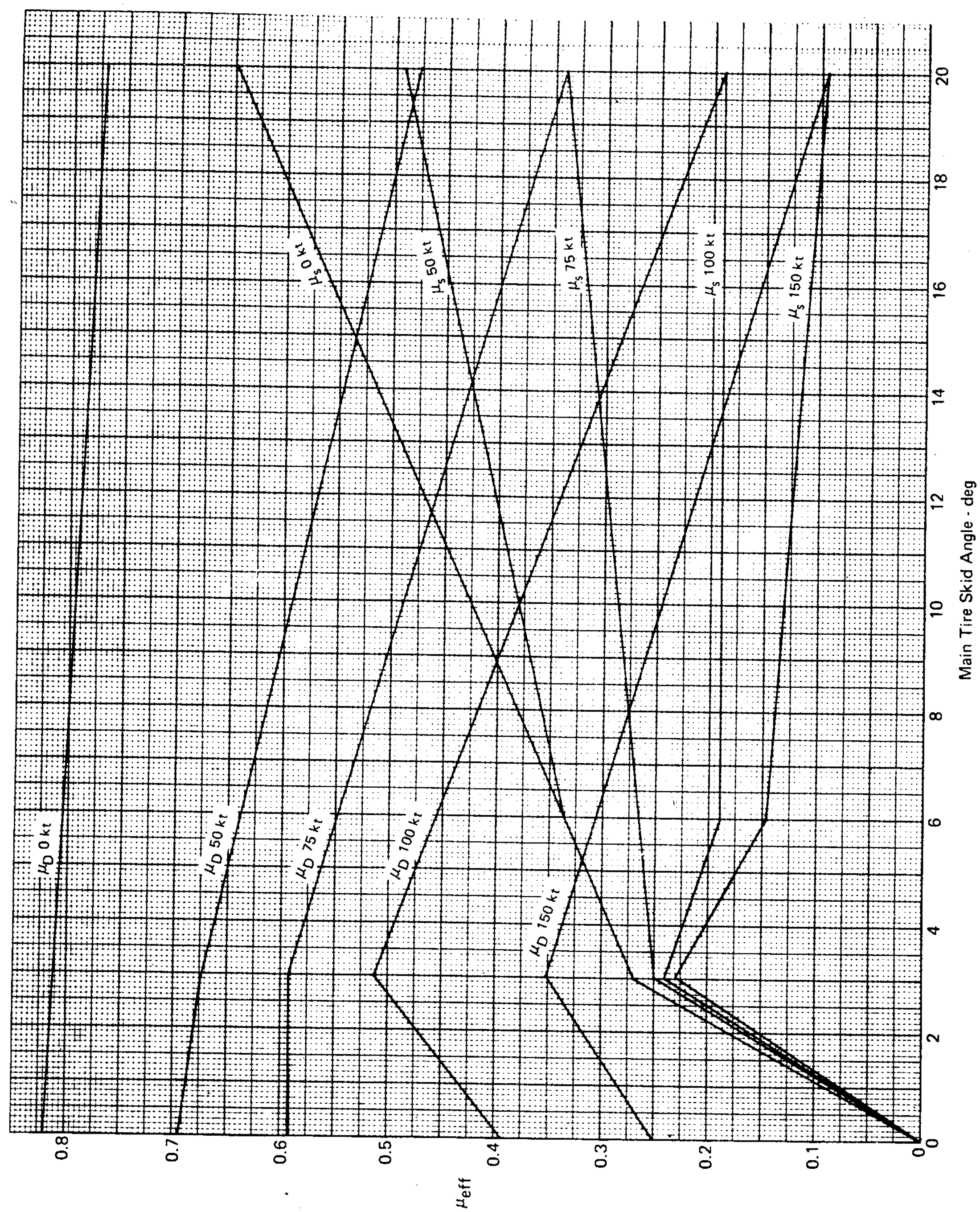

FIGURE 7-6

DC-9 MAIN TIRE CORNERING/BRAKING COEFFICIENT - DRY RUNWAY

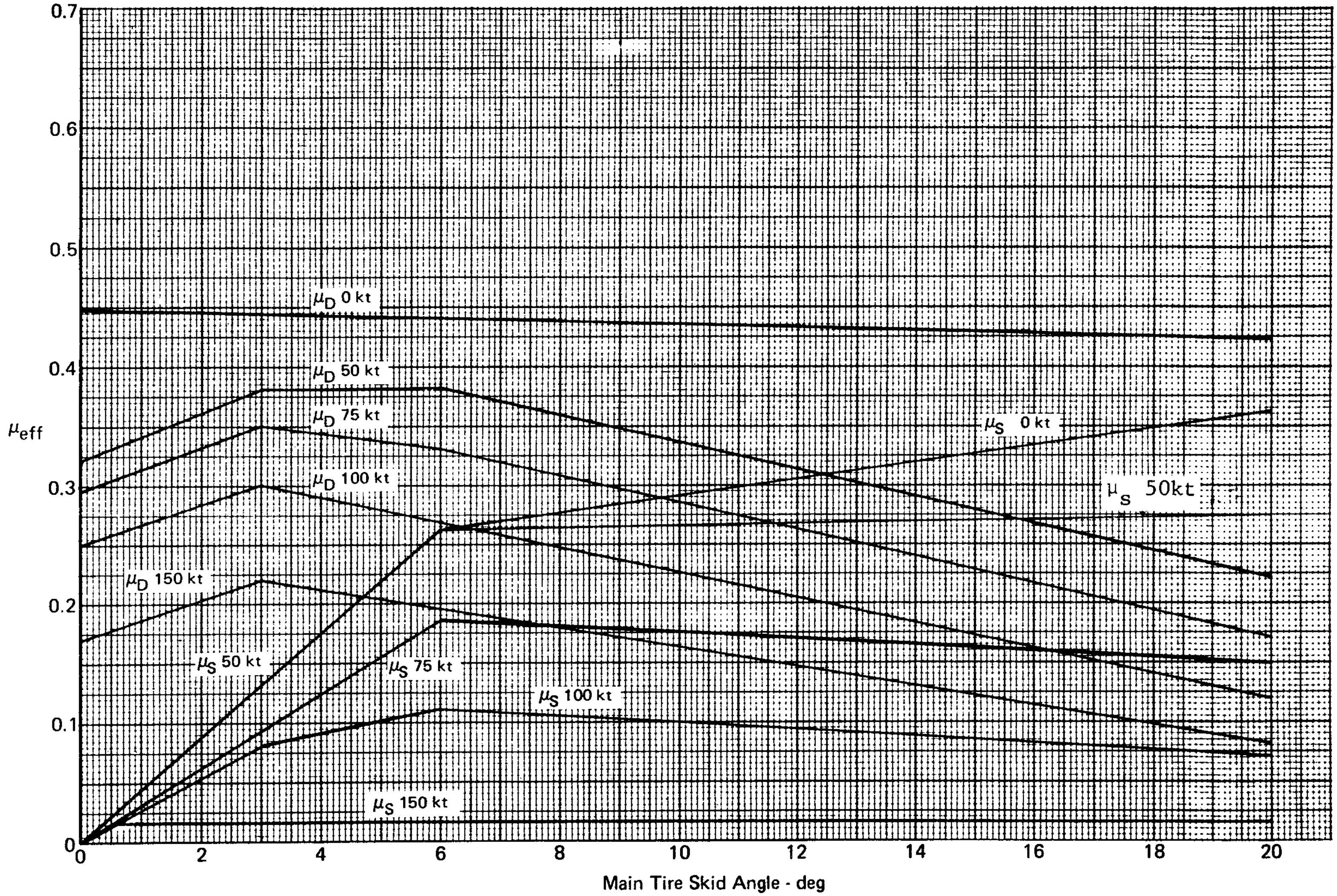

FIGURE 7-7
DC-9 MAIN TIRE CORNERING/BRAKING COEFFICIENT - WET RUNWAY

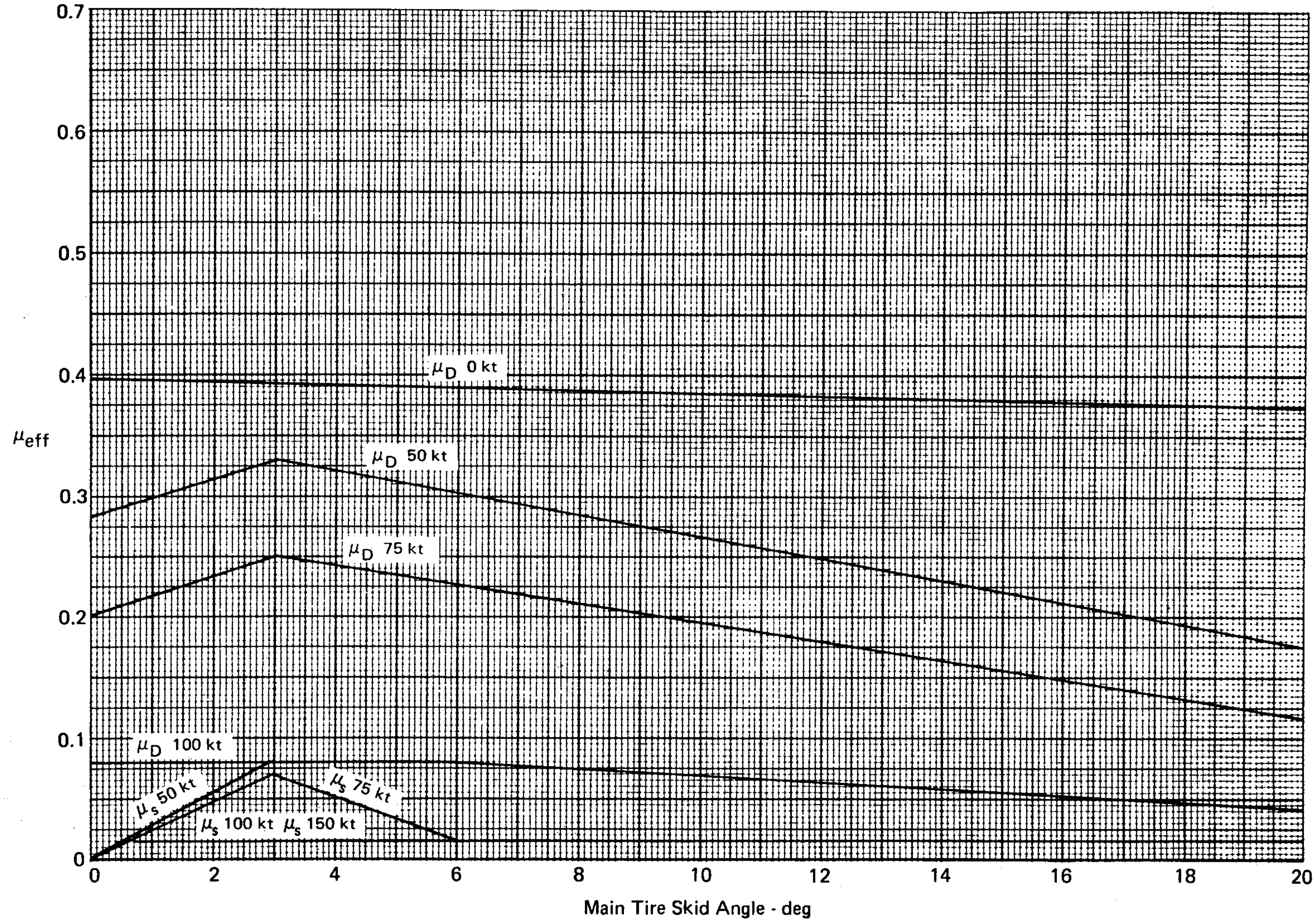

FIGURE 7-8
DC-9 MAIN TIRE CORNERING/BRAKING COEFFICIENT - FLOODED RUNWAY

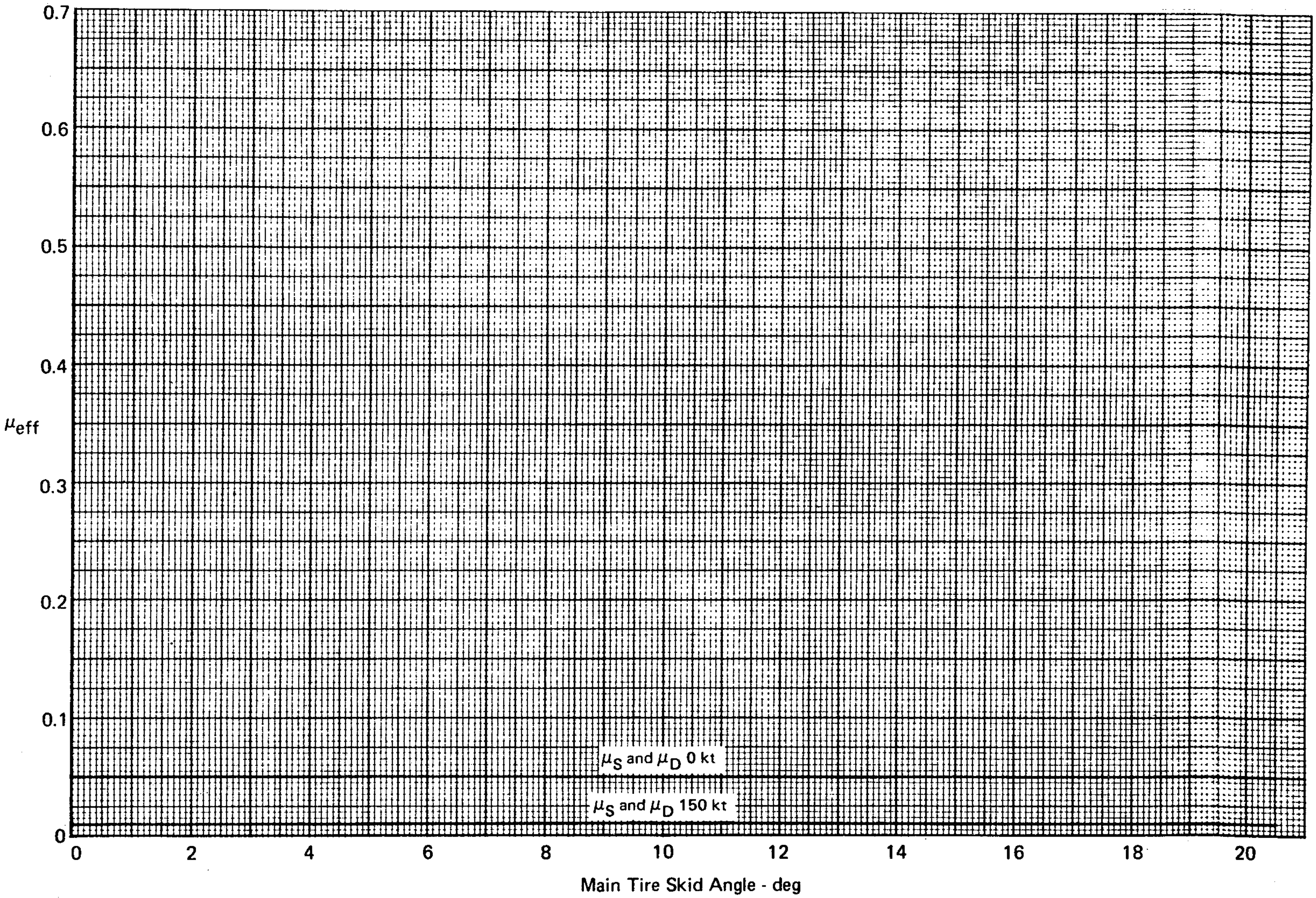

FIGURE 7-9
DC-9 MAIN TIRE CORNERING/BRAKING COEFFICIENT - ICY RUNWAY

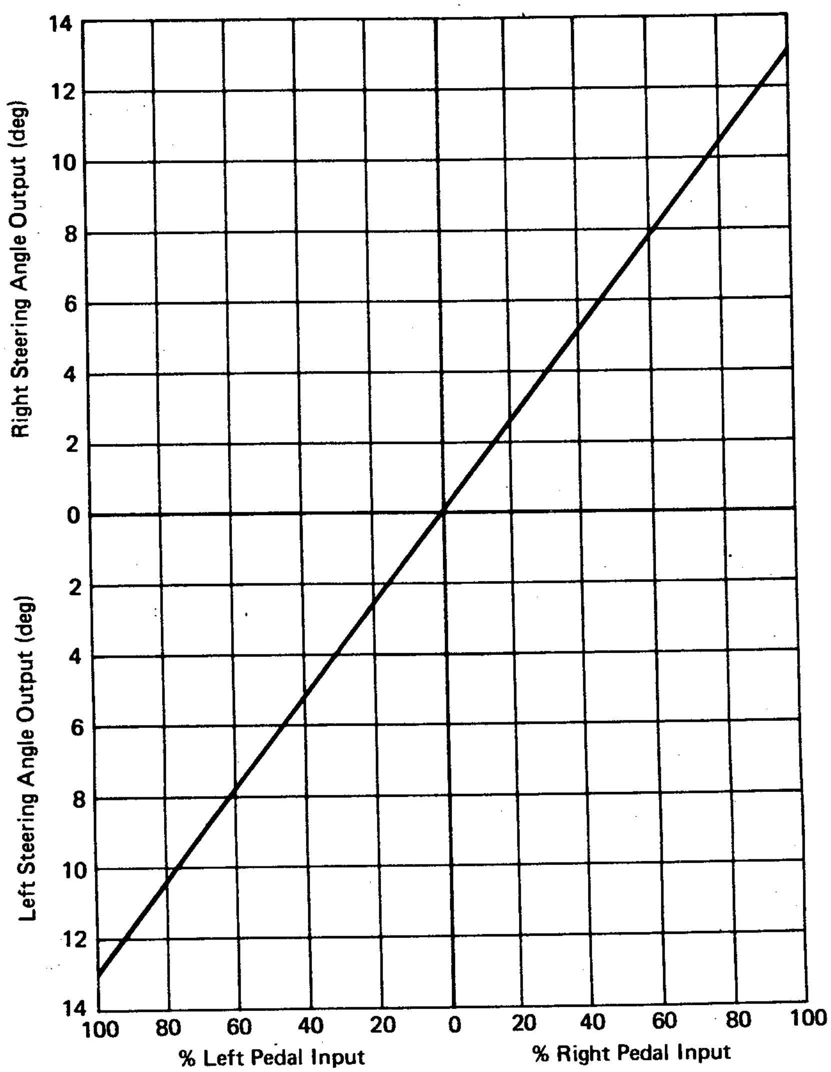

FIGURE 7-10
DC-9 STEERING RATIO